MEMBER

REPORT

[*China*]

ESCAP/WMO Typhoon Committee
18th Integrated Workshop
ESCAP - UN Conference Center, Bangkok, Thailand
28 November – 1 December 2023

CONTENTS

I. Review of Tropical Cyclones Affecting China since Last Session of ESCAP/WMO Typhoon Committee

1.1 Meteorological and Hydrological Assessment

Following the ending of last La Niña event which occurred from September 2021 to March 2023, the sea surface temperature (SST) in the equatorial central-eastern Pacific continued to increase significantly. The tropical Pacific entered an El Niño state as a result of rapid and substantial changes in oceanic and atmospheric conditions since this May. While with the warming equatorial central-eastern Pacific, the west tropical Pacific persisted warmer than normal ever since. As a response, the subtropical high over the northwest Pacific Ocean (hereinafter referred to as WPSH) kept weak eastward from Winter to early Spring and was strengthening since May, resulting in depressed convection and less-than-normal tropical cyclones (TCs) generation in the period.

In mid and late summer, a typical WPSH broke out two centers locating over the eastern South China and the southern Philippine Sea basin, the southeasterly winds prevailed over China's offshore area as the TC steering flows. Therefore, it was conducive to the track of the typhoon to the northwest and the typhoon is easy to move northward. On the other hand, TCs activities were affected by the large-scale atmospheric circulations. Due to the local instability of atmospheric circulations over the northwest tropical Pacific, the WPSH shifted southward or northward

several times, which to some extent resulted in the complicated and changeable TC tracks.

From 1st January to 16th October 2023, the Western North Pacific (WNP) and the South China Sea (SCS) have witnessed the formations of 15 TCs, which is 5.4 less than the average number of multiple years during the same period (20.4). Out of these 15 TCs, five of them made landfall in China, which is 1.9 less than the average number (6.9) for the same period. Typhoon Talim (2304) made landfall in Zhanjiang, Guangdong, and Beihai, Guangxi, on 17th and 18th July. Typhoon Doksuri (2305) made landfall in Jinjiang, Fujian, on 28th July. Typhoon Saola (2309) made landfall in Zhuhai and Yangjiang, Guangdong, on 2nd September. Typhoon Haikui (2311) made landfall in Taitung, Taiwan, Dongshan, Fujian, and Raoping, Guangdong, on 3rd and 5th September respectively. Typhoon Koinu (2314) made landfall in Pingtung, Taiwan, on October 5th. Typhoon Sanba (2316) made landfall in Dongfang, Hainan, and Suixi, Guangdong, on 19th and 20th October respectively.

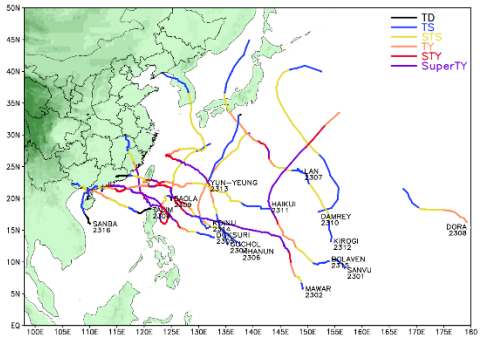

Fig. 1.1 Tracks of TCs over the WNP and the South China Sea from 1st January to 31th October 2023.

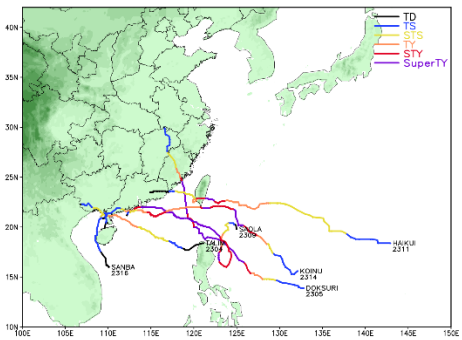

Fig1.2 Tracks of TCs that made landfall over China from 1st January to 31th October 2023.

1.1.1 Characteristics of TCs in 2023

In 2023, typhoon activity has displayed several features as follows: a eastward shift in typhoon genesis area, a reduction in the number of genesis and landfalls, increased intensity, and a heightened occurrence of extreme heavy rainfall events caused by TCs.

1) Eastward Origins

Up to 31th October, the average genesis location for the 16 TCs this year is 15.5°N, 141.2°E. This shows a southward deviation of 0.6 degrees in latitude and an eastward deviation of 4.9 degrees in longitude compared to the annual average of 16.1°N, 136.3°E (Fig. 1.3).

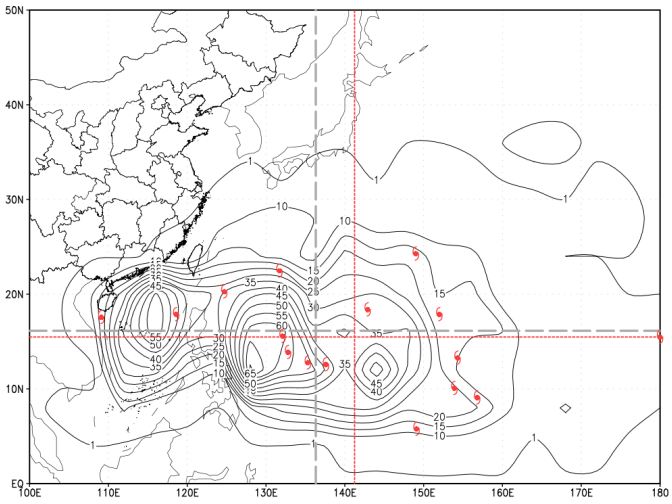

Fig. 1.3 1949-2021 WNP and SCS tropical cyclone source region density distribution (resolution: 2.5°×2.5°) and genesis location of tropical cyclones forming from 1st January to 31th October 2023.

2) Less TCs Generated with Higher Average Intensity

As of October 31, there have been 16 TCs generated in the WNP and the SCS, which is 5.9 less than the average for the same period in multiple years. With the exception of slight exceeding in April and

August, the number of TCs in other months is under the average. Specifically, there is a deficit of 3.0 TCs in September and 1.5 TCs in October. The average maximum intensity for TCs this year is 45.1m/s, which is 7.0m/s stronger than the annual average of 38.1m/s (Fig. 1.4).

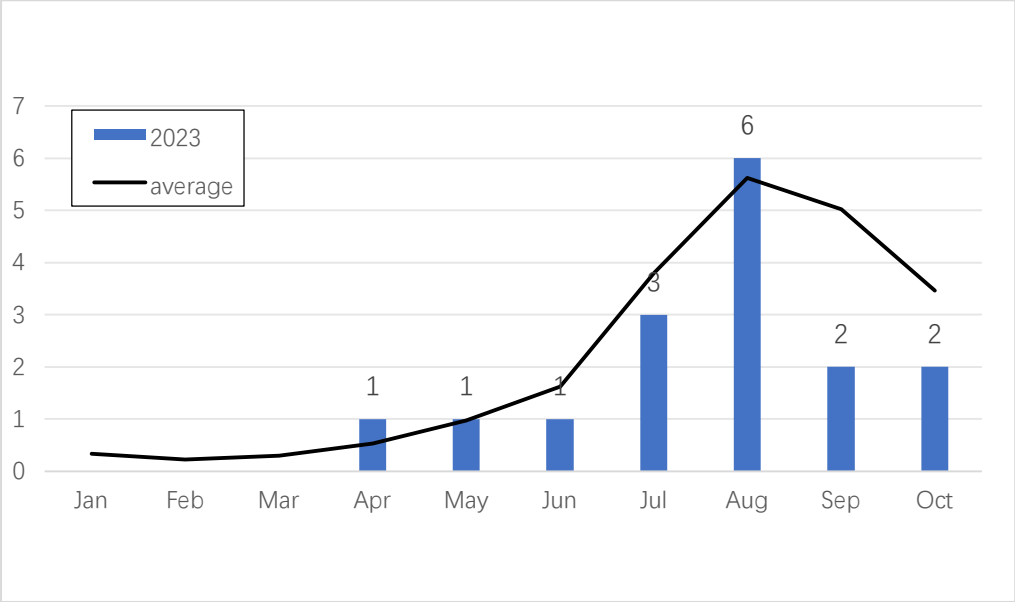

Fig. 1.4 1991-2020 Monthly multi-year average number of TCs (black solid line) and monthly number of TC generation from January to October in 2023 (blue bar).

3) Fewer Landfall TCs, but Significantly Stronger in Landfall Intensities

In 2023, there have been a total of 6 TCs making landfall in China, which is 1.1 less than the average number (7.1) within the same period in previous years. The landing areas include the provinces of Guangdong, Fujian, and Taiwan. The average landfall intensities of these 6 landfalling TCs is 41.8m/s (for those make landfall more than 1 time, only their first landfalls were taken into account), remarkably stronger by 9.1m/s compared to the annual average of 32.7m/s.

4) Frequent Extreme Typhoon-Related Heavy Rainfall Events

During the landfall of Typhoon Doksuri, it brought heavy rainfall to Zhejiang and Fujian provinces. After the typhoon's landfall, it moved northward, and its circulation lingered over land for an extended period, resulting in history-breaking extreme heavy rainfall in wide range of several regions, including North China and the Huanghuai region. When Typhoon Saola made landfall, it interacted with cold air, causing widespread heavy rainfall in Guangdong and Guangxi provinces. Moreover, Typhoon Haikui's remnant had a long-maintained impact on South China, induced breaking historical records for precipitation of several stations in Fujian, Guangdong, and Hong Kong.

1.1.2 Precipitation of TCs Affecting China

Up to 31th December, 2023, a total of 7 TCs have landed in China in 2023. The Haihe River experienced basin-wide super flood and 258 rivers across China witnessed floods exceeding the warning level. Among them, Typhoon Doksuri (2305) has the greatest impact, mainly presenting the following three characteristics:

1) Widely-Ranged Rainfall

From 27th July to 1st August, 9 provinces including Fujian, Zhejiang, Anhui, Henan, Shandong, Hebei, Beijing, Tianjin and Shanxi experienced heavy rainfall due to the joint influence of the Typhoon

Doksuri and the cold air, among which some part of Fujian, Zhejiang, Henan, Shandong, Hebei, Beijing, Tianjin and Shanxi provinces witnessed extremely heavy rainfall.

2) Severe Rainfall Intensity

The maximum cumulative rainfall during the process is 841mm in the Jiaoxi station of Putian of Fujian, 791mm in the Duofeng station of Hebi of Henan, 715mm in the Lingxi station of Baoding of Hebei, 654mm in Wuyang of Wenzhou of Zhejiang, 608mm in Huaishupu of Yangquan of Shanxi, and 594mm in the Wangjiayuan Reservoir of Beijing.

3) History-breaking Floods

A basin wide super flood occurred in the Haihe River Basin, including the Daqing River and Ziya River, and the Yongding River. 31 rivers experienced floods exceeding the warn level with a range of 0.04-4.38m, 7 rivers experienced floods exceeding the guaranteed level with a maximum range of 0.35-3.18m, and 8 rivers claimed the historical breaking records.

1.1.3 TCs Affecting China

1) Typhoon TALIM (2304)

Typhoon Talim formed over the central part of the South China Sea at 00:00UTC on 15th July. It gradually intensified as it moved in a west-

northwest direction. By 18:00UTC on 15th July, it reached severe tropical storm threshold, and further intensified into a typhoon by 23:00UTC. Its peak intensity reached 40m/s. On the 16th July, around 14:20UTC, Talim made landfall as a typhoon along the coast of Nanshan Island, Zhanjiang, Guangdong Province with intensity of 38m/s, and central pressure 965hPa. It then continued its westward track, passing through the Leizhou Peninsula and entering the Beibu Gulf. Around 21:45UTC on the 17th July, Talim made a second landfall in of Beihai, Guangxi, as a severe tropical storm (25m/s, 980hPa). Subsequently, Talim continued to weaken and was finally downgraded to a tropical depression within Guangxi.

Due to the impact of Talim, from 16th to 19th July, accumulated rainfall in Hainan Island, central and western parts of Guangdong, southeastern region of Guangxi, and other areas reached 100-220mm. The western regions of Hainan Island, the southwestern areas of Guangdong, and the southeastern areas of Guangxi received 250-460mm of rainfall. In some coastal areas, there were gusts of wind reaching Beaufort scale (Bft)-7 to 10, with the western parts of Guangdong, the southeastern regions of Guangxi having Bft-12 to 13, and some stations recording Bft-14 to 15.

Affected by TC's rainfall, 4 small and medium-sized rivers in Guangdong and Guangxi provinces experienced floods exceeding the warning level with a range of 0.06-0.59m. In addition, a total of 14 tidal

stations in Guangdong, Guangxi, and Hainan provinces exceeded the warning level with a range of 0.01-0.24m.

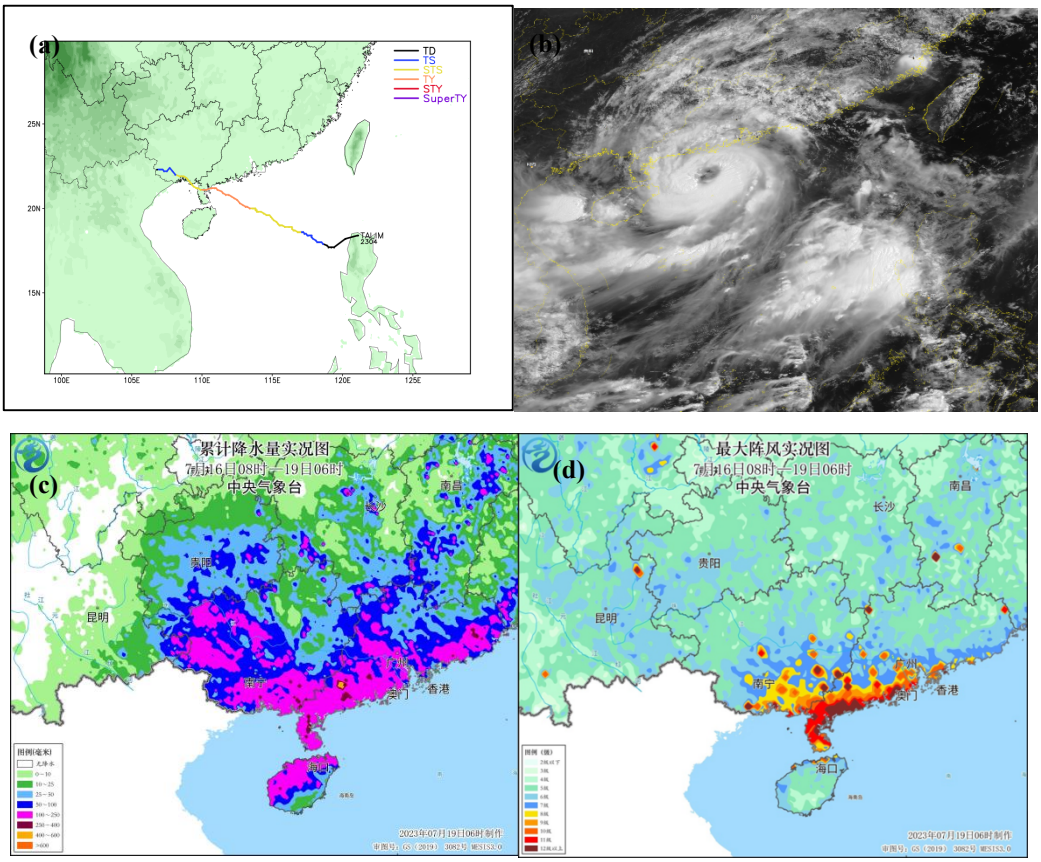

Fig. 1.5 Typhoon Talim track (a), FY-4B Satellite image at 02:47(UTC) 17th July (b), accumulated rainfall (c) and real-time gust (d).

2) Super Typhoon DOKSURI (2305)

Super Typhoon Doksuri formed over the open ocean to the east of the Philippines at 00:00UTC on 21th July. It initially moved in a westward direction. By 21:00UTC on 22th July, then it strengthened into a severe tropical storm, and by 09:00UTC on 23th July, it further intensified into a typhoon. Thereafter, it moved in a northwesterly direction with rapidly intensifying. At 00:00UTC on 24th July, it reached

the status of a severe typhoon and by 12:00UTC within the same day, it upgraded to a super typhoon. It maintained super typhoon status for a prolonged period, lasting for 56hours, before passing through the Bashi Channel between 25th and 26th July, skirting over north of Luzon Island of the Philippines.

Upon entering the SCS, Doksuri shifted its direction to the north-northwest and downgraded to a severe typhoon. By 09:00UTC on 27th July, it regained super typhoon intensity and, around 01:55UTC, it made landfall along the coastal areas of Jinjiang, Fujian, as a severe typhoon (50m/s, 945hPa). It was the strongest TC to make landfall over the Chinese mainland this year and the second-strongest to strike Fujian since 1949. After making landfall, Doksuri rapidly weakened and continued northward. It further weakened into a tropical depression in Anhui Province. Its remnant circulation moved further north and remained over land for an extended period, caused widespread heavy rainfall in North China.

The circulation of Doksuri's remnant has for over 70 hours after making landfall, significantly longer than the average duration of landfalling typhoons in China (20 hours).

From 26th to 30th July, parts of Fujian, Zhejiang, Taiwan, and other regions experienced accumulated rainfall of 200-350mm. Quanzhou, Putian, Fuzhou, and Ningde in Fujian, as well as Wenzhou, Lishui,

Taizhou, and Ningbo in Zhejiang, witnessed local accumulations of 400-861mm, with local positions in Pingdong, Taiwan receiving more than 1400mm of rainfall. In eastern Fujian, eastern Zhejiang, Taiwan, and other areas, gust reached Bft-8 to 10, and in some locations, it escalated to Bft-11 to 16. Five national observation stations in Fujian's Quanzhou, Putian, and Fuzhou experienced record-breaking daily rainfall.

Under the influence of Doksuri's residual circulation when it moved northward, regions in northern China, including North China and the Huaihe River Basin, experienced extreme rainfall. This resulted in rainstorms, large-scale landslides, and severe urban flooding in parts of Beijing, Tianjin, Hebei's Baoding, and Shijiazhuang, leading to significant damage with vehicles and houses destroyed, multiple roads blocked, bridges collapsed.

Due to the heavy rainfall caused by Doksuri, a basin-wide super flood occurred in the Haihe River Basin, including the Daqing River and Ziya River, and the Yongding River. 31 rivers experienced floods exceeding the warning level with a range of 0.04-4.38m, 7 rivers experienced floods exceeding the guaranteed level with a range of 0.35-3.18m, and 8 rivers claimed the historical records.

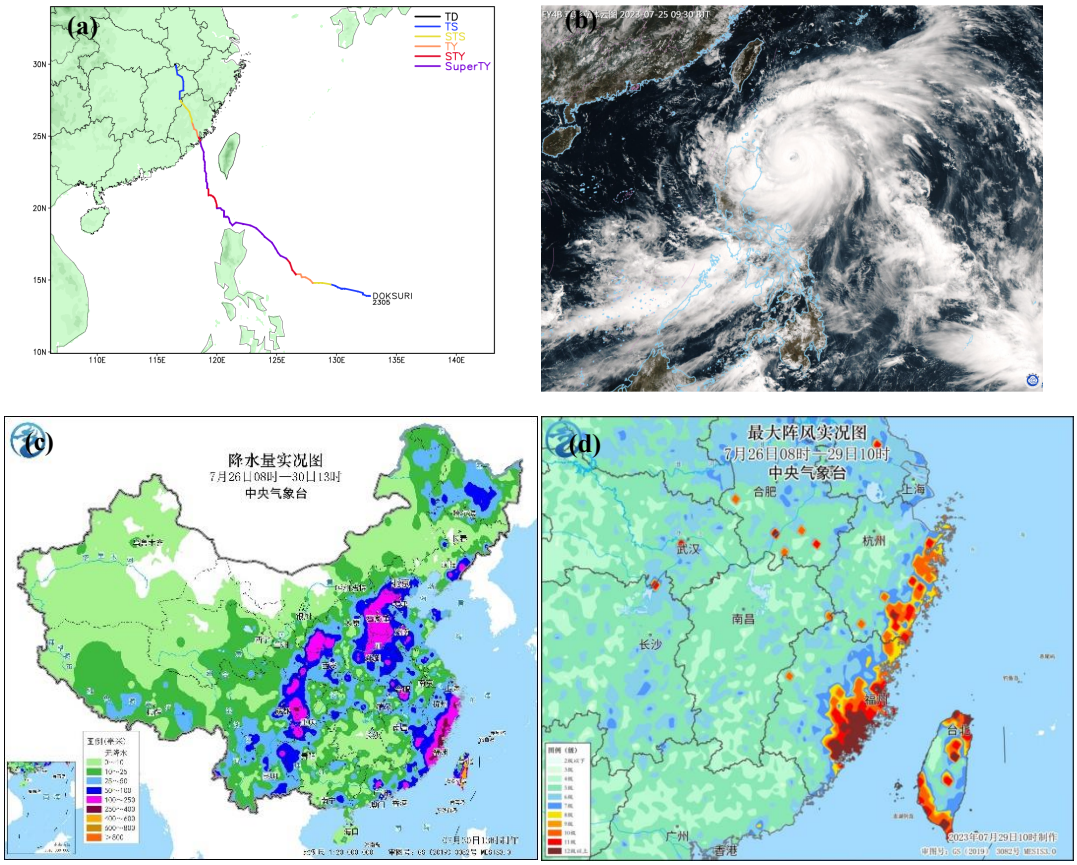

Fig. 1.6 Super Typhoon Doksuri track (a), FY-4B Satellite image at 01:30(UTC) 25th July (b), accumulated rainfall (c) and real-time gust (d).

3) Super Typhoon KHANUN (2306)

Super Typhoon Khanun formed in the WNP on 27th July at 18:00UTC. It initially moved in a northwesterly direction, subsequently undergoing a rapid intensification process from 29th July at 18:00UTC to 31th July at 06:00UTC when it rapidly intensified from a severe tropical storm to a super typhoon, with a maximum 24-hour intensity change of 15m/s.

Following this phase, Khanun underwent two significant track changes. From 3rd to 4th August, it turned towards the east, and from 6th to 8th August, it changed to a north-northwesterly moving, east of the

Ryukyu Islands. On or around 10th August at 02:00UTC, Khanun made landfall along the coast of Gyeongsangnam-do in Republic of Korea as a severe tropical storm with maximum sustained winds of 28m/s and a minimum central pressure of 975hPa. It traversed the Korean Peninsula from south to north, resulting in heavy precipitation in both Republic of Korea and Democratic People's Republic of Korea (DPRK).

Around 11th August at 09:00UTC, Khanun entered the northern Yellow Sea and, at 15:00UTC, made landfall once more in Zhuanghe, Liaoning Province, China, as a tropical depression with a maximum wind speed of 12m/s and a minimum central pressure of 1000hPa. Subsequently, it rapidly weakened and then dissipated over land. Due to its influence, the cumulative rainfall in northeastern China reached 100-200mm.

Khanun had an extended life span of 15 days, significantly longer than the average lifespan of 6.2days for TCs in the WNP. The two large-angle turnings in its track after entering the East China Sea not only introduced considerable forecast uncertainties but also posed challenges to the disaster defense efforts in the coastal provinces and cities.

Due to the heavy rain caused by Khanun, 19 rivers in Heilongjiang and Jilin provinces including Suifen River, Muling River, Woken River and Gaya River experienced floods exceeding the warning level with a

range of 0.01-3.54m, 3 rivers experienced floods exceeding the guaranteed level with a range of 0.09-2.09m.

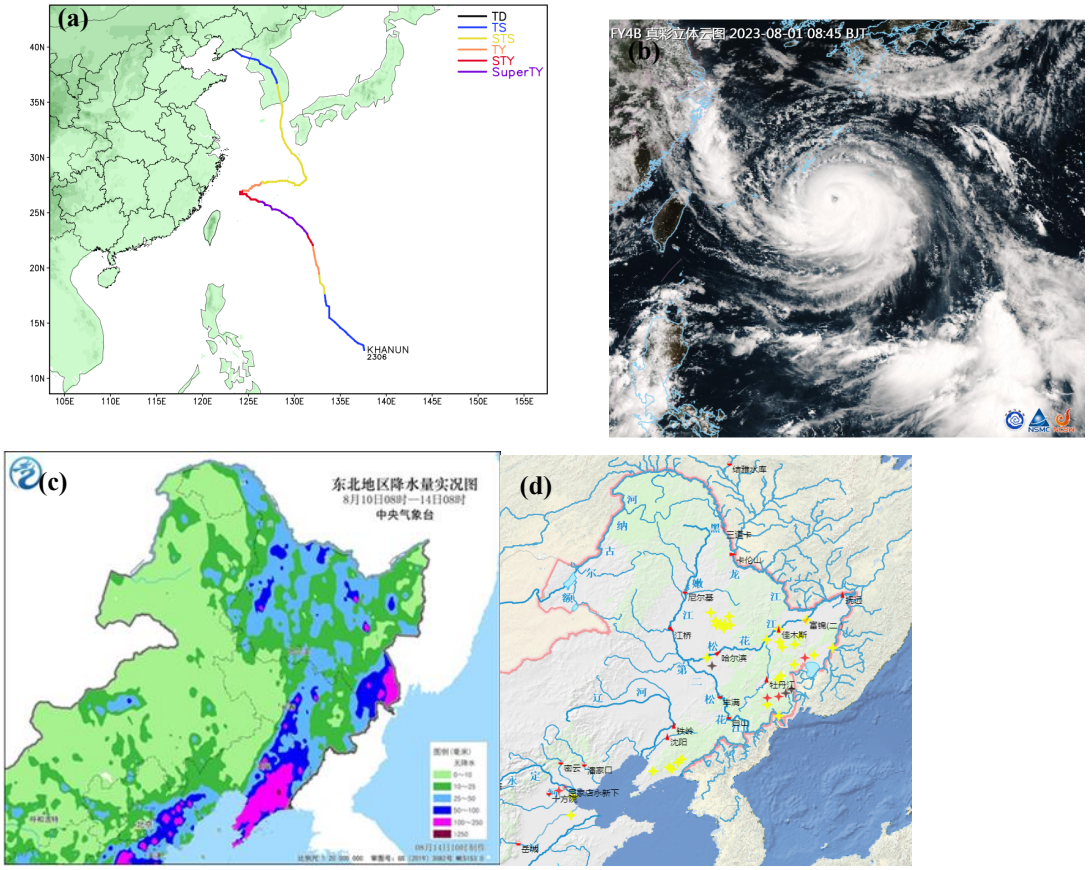

Fig. 1.7 Super Typhoon Khanun track (a), FY-4B Satellite image at 00:45(UTC) 1st August (b) and accumulated rainfall (c), rivers exceeding the warning level (d).

4) Super Typhoon SAOLA (2309)

Super Typhoon Saola formed over the open ocean east of the Bashi Channel on 24th August at 06:00UTC. By 25th August at 18:00UTC, it upgraded into a typhoon. By 26th August at 06:00UTC, Saola further intensified into a strong typhoon. Within the following 24hours, Saola 's intensity increased by 25m/s, reaching it to the status of a super typhoon. It maintained the status of super typhoon for 12hours until 27th August at

06:00UTC when it remained a severe typhoon. Since its formation, Saola had been predominantly moving in a south-southwesterly to southerly direction.

However, during the last period, Saola began to change its course, rotating counterclockwise in the vicinity of the waters east of Luzon Island, gradually shifting in a west-northwesterly direction, eventually crossing the Bashi Channel and nearing the coast of Guangdong. On 29th August at 09:00UTC, Saola once again intensified into a super typhoon in the second time and maintained this status for a prolonged period, lasting 82hours. When it reached the vicinity of the Pearl River's estuary, it weakened to a strong typhoon. On 1st September at 19:30UTC, Saola made landfall in Zhuhai, Guangdong, with a maximum sustained wind speed of 45m/s and a minimum central pressure of 950hPa. Afterward, it rapidly decreased, on 2nd September at 05:50UTC, and made its second landfall as a severe tropical storm in Hailing Island, Yangjiang, Guangdong, with a maximum sustained wind speed of 28 m/s and a minimum central pressure of 982hPa. Upon entering the Beibu Gulf on 3rd September, it further weakened into a tropical depression and dissipated.

Saola was the second-strongest typhoon to make landfall in the Pearl River Delta region (second only to Typhoon Hato in 2017, which made landfall at Zhuhai, Guangdong, as a severe typhoon with maximum

sustained winds of 48m/s).

From 31th August to 3nd September, cumulative rainfall in eastern Guangxi, most parts of Guangdong, southeastern Fujian, central and eastern Taiwan reached 60-120mm. In specific areas, such as Zhangzhou and Quanzhou in Fujian, Jieyang, Shanwei, Huizhou, Shenzhen, Zhuhai, Jiangmen, Yunfu, Yangjiang, Zhaoqing, Maoming, and Dongguan in Guangdong, Hong Kong, Yulin, Wuzhou, and Guigang in Guangxi, and eastern Taiwan, rainfall ranged from 150-280mm. Some location observation stations experienced even higher rainfall, with areas like Zhangzhou in Fujian, Shanwei, Huizhou, Zhuhai, Jiangmen, Yunfu, Maoming, and Taitung in Taiwan seeing 300-457mm. Due to the combined influence of Saola and a cold air mass moving southward, mainland regions in eastern China and most parts of southern China experienced wind gusts of Bft-6 to 7. In specific coastal areas, including Guangdong's central and eastern regions, eastern Guangxi, and northern Taiwan, wind gusts reached Bft-8 to 10, with some locations experiencing wind gusts exceeding Bft-2. Strong winds of Bft-10 or more mainly occurred near the coastlines and coastal regions due to Saola's relatively small size, with less penetration of strong winds into inland areas.

According to the National Disaster Reduction Center, Saola resulted in 787,000 people being affected in Guangdong and 158,000 people affected in Fujian. Additionally, the typhoon led to the suspension of over

120 passenger train services.

Due to the heavy rain caused by Saola, 37 small and medium-sized rivers in Fujian, Guangdong, Guangxi and Hainan provinces have experienced floods exceeding the warning level with a range of 0.01-3.53m, and Luoding River in Guangdong province claimed the historical record since 1958.

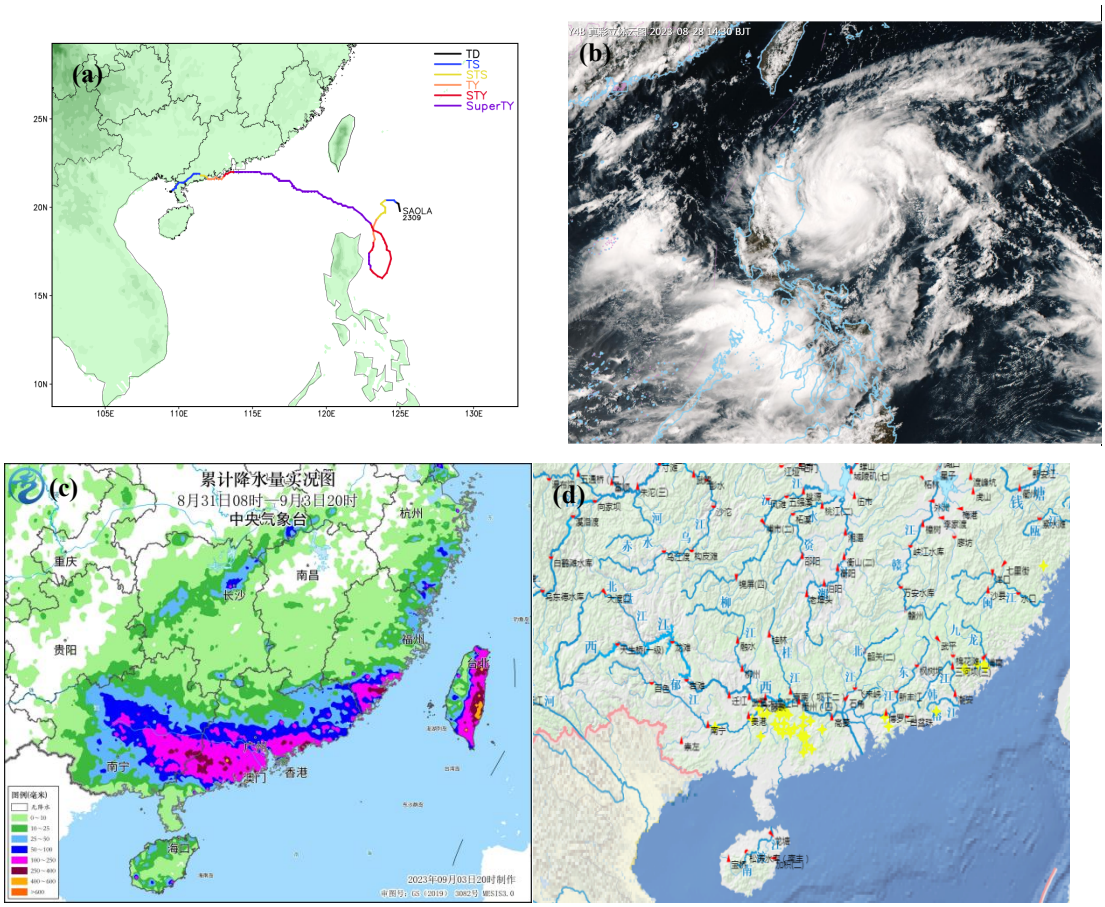

Fig. 1.8 Super Typhoon Saola track (a), FY-4B Satellite image at 06:30(UTC) 28th August (b) and accumulated rainfall (c), rivers exceeding the warning level (d).

5) Super Typhoon HAIKUI (2311)

Super Typhoon Haikui originated on the open waters of the northwestern Pacific Ocean on 28th August at 00:00UTC. It began moving towards the west and west-northwest direction, gradually

increasing in intensity. By 29th August at 06:00UTC, Haikui had strengthened into a severe tropical storm. At 1st September 06:00UTC, it further intensified into a typhoon and then reached severe typhoon status by 2nd September at 15:00UTC. As it approaching Taiwan, Haikui rapidly intensified, reaching super typhoon status by 3rd September at 02:00UTC. Later that day, at 07:30UTC, it made landfall on the coastal areas of Taitung, Taiwan, with maximum sustained winds of 50m/s and a minimum central pressure of 940hPa.

After landfall, Haikui gradually weakened as it moved westward, crossing Taiwan and entering the Taiwan Strait. Near the southwestern coast of Taiwan, it shortly lingered before continuing its westward course. On 4th September, Haikui made landfall twice, first in Dongshan County, Fujian, at 21:20UTC, with maximum sustained winds of 20m/s and a minimum central pressure of 995hPa, and later in Raoping, Guangdong, at 22:45UTC, with maximum sustained winds of 18 m/s and a minimum central pressure of 995hPa. By 5th September at 21:00UTC, it had weakened to a tropical depression. On 6th September at 09:00UTC, the National Meteorological Centre stop issuing advisories for the typhoon. Following the cessation of advisories. The remnants of Haikui's circulation continued to move slowly in a southwest direction, passing through the Pearl River Delta and parts of Guangdong, Guangxi, Jiangxi, and Hunan, maintaining its influence.

The circulation and remnants of Haikui had a prolonged impact, affecting Fujian for 5days from 3th to 7th September, Guangdong for 8 days from 4th to 11th September, and Guangxi for 6 days from 8th to 13th September.

From 3th to 13th September, eastern Fujian, southern Guangdong, eastern and southern Guangxi, Hainan, southern Hunan, southern Jiangxi, Macau, and Taiwan experienced cumulative rainfall of 100-300mm. Specific areas, including eastern Fujian, central and western Guangdong, southern Guangxi, Hong Kong, and eastern Taiwan, recorded rainfall ranging from 400-902mm. In some places, such as eastern Taiwan's Hualien, rainfall exceeded 1100mm. Between the 7th and 8th of September, the Pearl River Delta region experienced heavy rainfall. Shenzhen, on average, received over 200mm of rain, while localities such as Luohu and Yantian recorded over 500mm of rain. Rainfall in Hong Kong and Kowloon exceeded 600mm. Close to 200mm of rain was recorded in Macau. From 3nd to 6th September, eastern and southern Taiwan, as well as coastal areas of eastern Fujian, experienced gusts of Bft-8 to 10, while certain coastal regions, including eastern Taiwan, and cities such as Fuzhou, Putian, and Quanzhou in Fujian, recorded gusts ranging from Bft-12 to 14. On 7th to 8th September, parts of central and eastern Guangdong, as well as Hong Kong and Macau, experienced gusts of Bft-6 to 8, with some coastal areas in Shenzhen recording gusts of

scale Bft-9 to 10.

During that period, 17 meteorological observation stations in Fujian, Guangdong, Guangxi, and Jiangxi experienced rainfall that exceeded historical September records, with 6 stations surpassing historical records. Shenzhen in Guangdong recorded 7 historical rainfall records for 2hours, 3hours, 6hours, 12hours, 24hours, 48hours, and 72hours since meteorological records began in 1952. The Hong Kong Observatory reported a maximum hourly rainfall of 158.1mm, the highest ever recorded in Hong Kong since 1884. Stanley, a location in the southeastern part of Hong Kong Island, registered 842mm of rainfall within 24hours, breaking records in Hong Kong.

Haikui had a significant impact on Fujian, Guangdong, Guangxi, as well as Hong Kong, Macau, and Taiwan. Several regions experienced urban and rural waterlogging, landslides, road interruptions, and more than 70 small and medium-sized rivers exceeded warning levels with floods. Mulanxi and Lanxi in Fujian experienced floods that exceeded safety levels, while Moyang River in Guangdong witnessed its highest flood in over a decade. Six small and medium-sized rivers, including the Shima River, a tributary of the Dongjiang in Shenzhen, also encountered riverbank flooding. In response to Haikui, schools in Fuzhou, Shenzhen, Zhuhai, Jiangmen, and other cities across Fujian and Guangdong temporarily suspended classes, and multiple train services were canceled.

Up to 13th September, around 3.01million people in Fujian, Guangdong, Guangxi, and other regions were affected by the typhoon. Tragically, 12 individuals lost their lives, and approximately 64,000 hectares of crops were affected. The direct economic losses amounted to 15.83billion RMB.

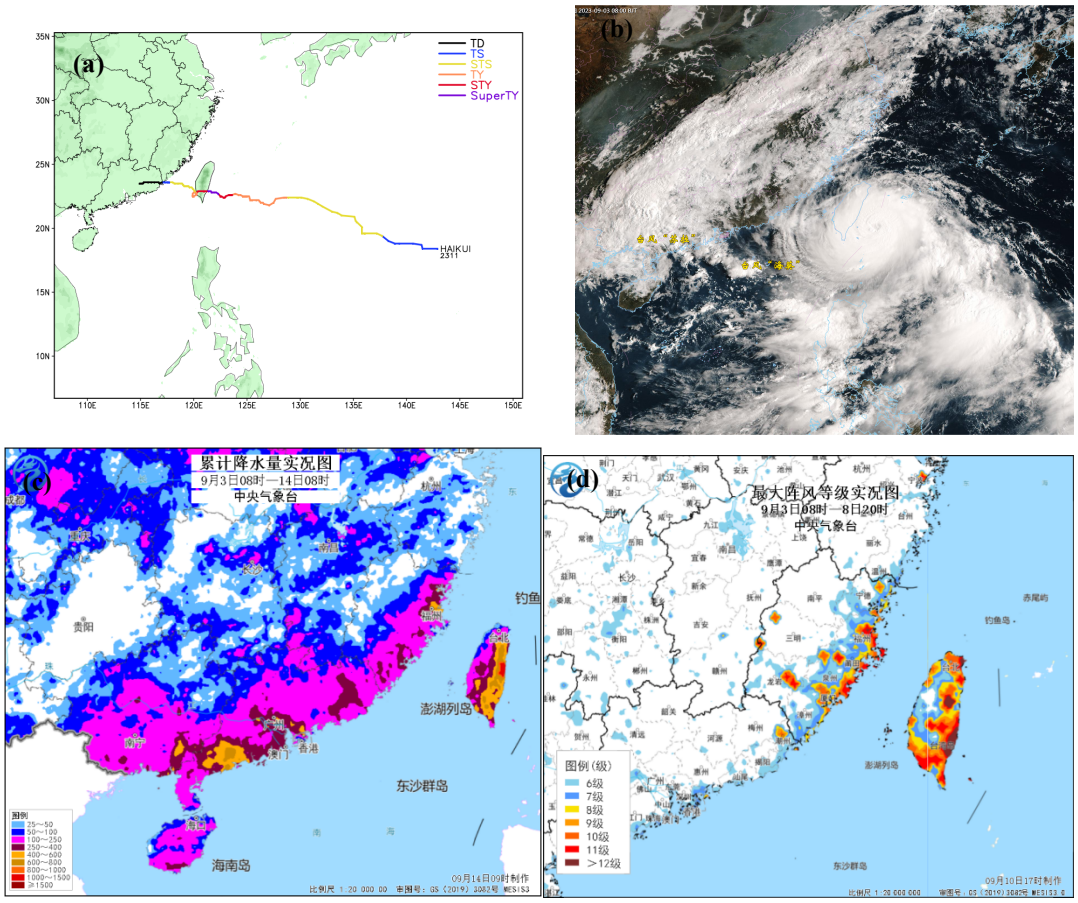

Fig. 1.9 Super Typhoon Haikui track (a), FY-4B Satellite image at 00:00(UTC) 3rd September (b), accumulated rainfall (c) and real-time gust (d).

6) Super Typhoon KOINU (2314)

Super Typhoon Koinu formed over the open waters of the Philippines on 29th September at 21:00UTC. It initially moved westward and gradually intensified. By 1st October at 03:00UTC, Koinu strengthened into a severe tropical storm and later intensified into a

typhoon at 12:00UTC. At 00:00UTC on 2nd October, it further strengthened into a severe typhoon. Over the course of 24 hours, Koinu intensified by 22m/s, reaching super typhoon status by 15:00UTC on the same day.

On 3rd October at 12:00UTC, Koinu weakened to a severe typhoon and began to move westward. As it approaching Taiwan, it regained super typhoon status at 14:00UTC on 4th October. At 00:20UTC on 5th October, Koinu made landfall in Pingtung, Taiwan, near the south cape of Taiwan, with a maximum sustained wind speed of 48m/s and a minimum central pressure of 945hPa.

Subsequently, Koinu rapidly weakened to a typhoon as it moved towards the coast of Guangdong. By 09:00UTC on 6th October, it re-intensified into a severe typhoon as it approached the inshore again. After maintaining this status for 40hours, Koinu gradually weakened to a typhoon and, by 09:00UTC on 9th October, had weakened to a tropical depression off the coast of Guangdong.

Due to the combined influence of Typhoon Koinu and a cold air mass, from 5th to 9th October, parts of Guangdong, Hong Kong, Macau, southeastern Fujian, and southeastern Zhejiang experienced accumulated rainfall of 50-250mm. In the southern part of the Pearl River Delta in Guangdong, some areas received 300-500mm of rainfall, with localized amounts exceeding 600mm in places like Zhuhai in Guangdong and

Hong Kong. Along the coasts of southern Zhejiang, southeastern Fujian, and the central and eastern regions of Guangdong, there were wind gusts ranging from Bft-7 to 9, with some areas reaching Bft-10 to 12. Near the islands in the Pearl River estuary, winds reached Bft-15. The heaviest rainfall in the Guangdong-Hong Kong-Macao Greater Bay Area primarily occurred on the 8th and 9th October.

Furthermore, from 4th to 9th October, the central and eastern parts of Taiwan received accumulated rainfall of 200-500mm, with localized amounts exceeding 650mm in Pingtung, Taiwan. Coastal areas in western and southern Taiwan experienced wind gusts of Bft-8 to 10, with some regions reaching Bft-11 to 12, and some areas in southern Taiwan experienced wind gusts of Bft-13 to 15.

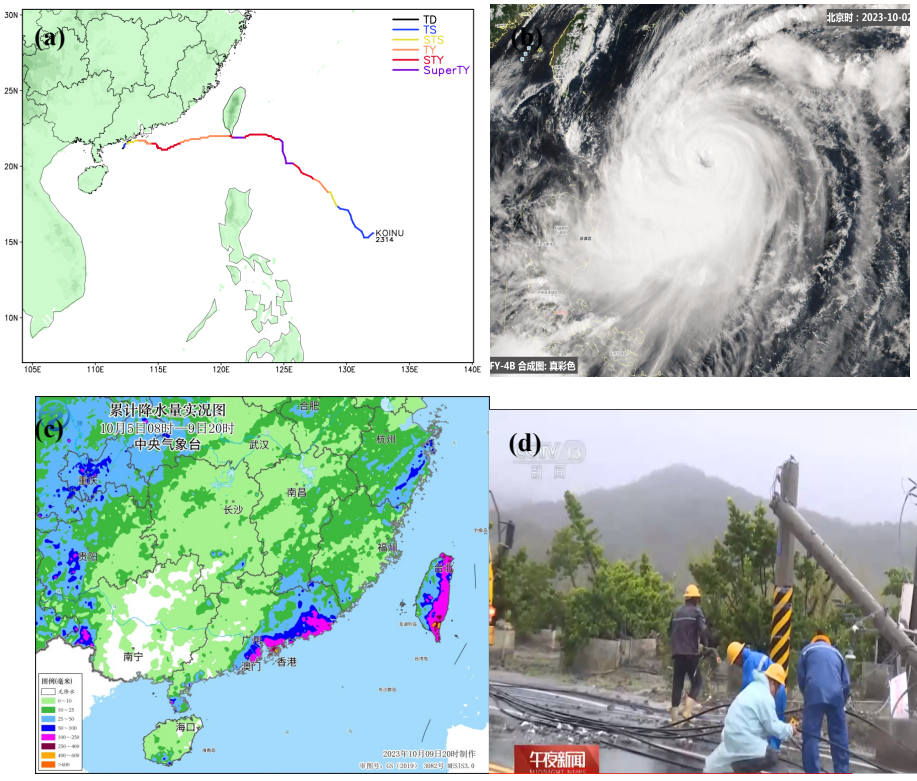

Fig. 1.10 Super Typhoon Koinu track (a), FY-4B Satellite image at 06:30(UTC) 2nd October (b), accumulated rainfall (c) and disaster influence (d).

7) Severe Tropical Storm SANBA (2316)

Severe Tropical Storm Sanba formed over the sea south of Hainan Island on 18th October at 06:00UTC. It then moved in a north-northwesterly direction and, after moving along the western coast of Hainan Island, and made landfall near Dongfang City, Hainan Province, around 01:00UTC on 19th October, with a maximum wind speed of 20m/s and a minimum central pressure of 998hPa. Shortly after landfall, Sanba re-entered the Beibu Gulf. As it moved in a north-northeast direction and approaching the coast of Guangxi, it intensified into a severe tropical storm around 13:00UTC on 19th October and maintained this category for about 7 hours, during which it exhibited a trend of stagnation. Around 00:00UTC on October 20, Sanba altered its course to the south and, soon after, made landfall as a tropical storm near Suixi County, Guangdong Province around 01:45UTC, with a maximum wind speed of 20m/s and a minimum central pressure of 998hPa. By 09:00UTC on 20th October, Sanba had weakened into a tropical depression in the waters west of Leizhou Peninsula. Around 11:40UTC on the same day, it made landfall as a tropical depression along the coast of Lin'gao County, Hainan Province, with a maximum wind speed of 13m/s and a minimum central pressure of 1010hPa.

Under the influence of Sanba, it's subsequent tropical depression and residual circulation, from 17th to 21th October, accumulative rainfall of 100-300 mm was observed in western Guangdong, southeastern Guangxi, and the central-eastern part of Hainan Island. Some areas in Guangdong, including Maoming, Zhanjiang, Yangjiang, Yunfu, and parts of Guangxi, such as Yulin, Beihai, and Qinzhou, received 350-650mm of rainfall. In some locations in northern Guangxi, rainfall reached up to 842mm. Additionally, the southern and eastern coasts of Hainan Island, the southwestern coast of Guangdong, and the southeastern coast of Guangxi experienced gusts of wind at Bft-7 to 10, with some locations reaching Bft-10 to 11. During that period, 9 national meteorological stations in Guangdong, Guangxi, and Hainan recorded daily rainfall exceeding the historical maximum for October. Notably, at the Yinhai Qiaogang Town, Yaping Meteorological Observation Station in Beihai, Guangxi, there was a 24-hour rainfall of 780.3mm, breaking the historical record for daily precipitation in Guangxi. The Dongping Meteorological Station in Bobai County, Yulin, registered a 24-hour rainfall of 522.1mm, surpassing the historical record for daily precipitation in Bobai County. In Aotou Town, Maonan District, Maoming, Guangdong, the maximum hourly rainfall reached 158.5mm, breaking the historical record for precipitation in Maoming.

Due to the heavy rain caused by Sanba, 60 small and medium-sized rivers in Guangdong and Guangxi provinces have experienced floods exceeding the warning level with a range of 0.05-3.83m, and 4 small rivers claimed the historical records.

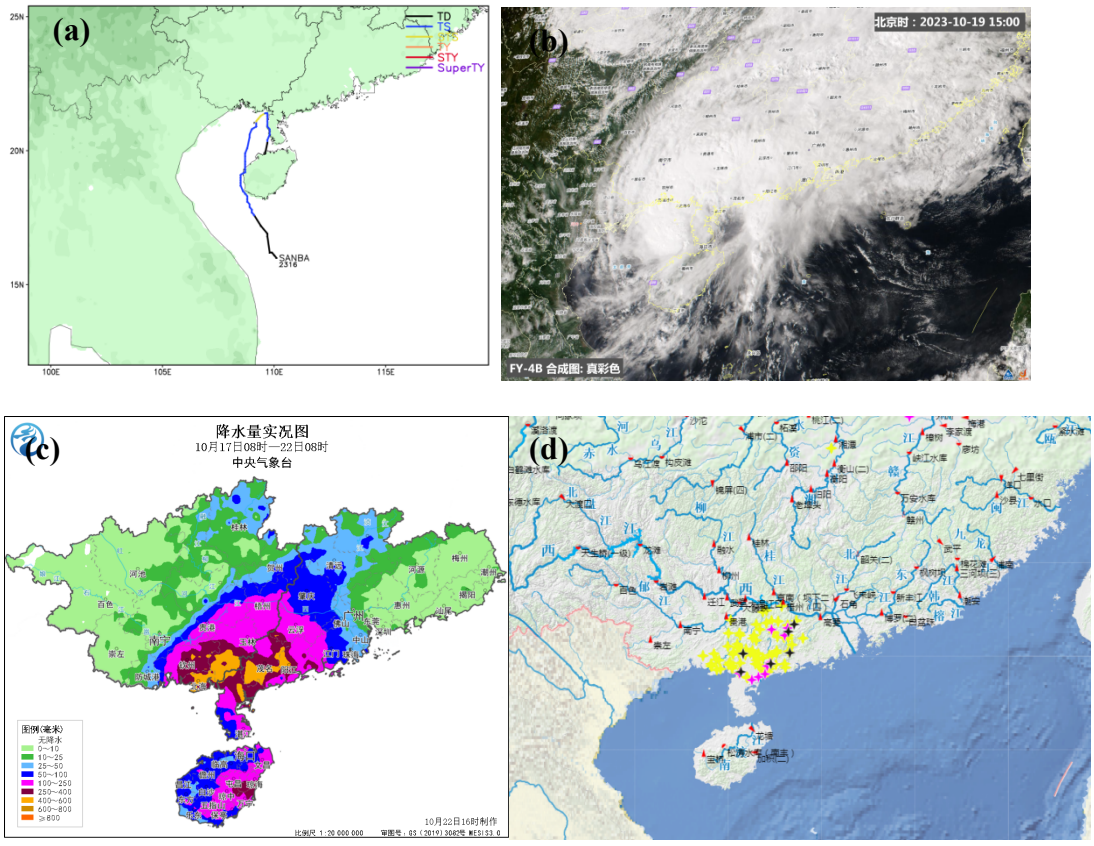

Fig. 1.11 Severe Tropical Storm Sanba track (a), FY-4B Satellite image at 07:00(UTC) 19th October (b) and accumulated rainfall (c), rivers exceeding the warning level (d).

1.1.4 Climatic Prediction of TCs

In March and May, the National Climate Center issued annual and seasonal forecasts on tropical cyclone (TC) activities in the SCS and WNP, including the number of TC generation, landfall frequency, distribution of tracks and intensity. The main methods are objective

method of dynamic-statistical combination and physical mechanism diagnosis.

1) Annual Prediction of TCs

In March of 2023, it was predicted that the number of TCs generated in the SCS and WNP in 2023 would be 24-27, close to normal (25, the average during 1991-2020 according to WMO, the same below). Among them, 6-8 TCs would land on China, close to normal (7). The overall intensity of the TCs would be medium to strong, and the path of the TCs activity would prevail westward and northwestward, with high possibility of northward heavy impact TCs.

Up to 31th October, there are 16 TCs genesis over WNP and SCS, with 6 TCs made landfall in China. The number of landed TCs is closed to climatologic average while the number of genesis is less than normal. The predicted frequency of landed TCs and TCs' intensity are both consistent with observation. Moreover, the prevail path of TCs was well predicted. However, there was a certain deviation between the prediction and observation on the number of TCs' genesis.

2) Prediction of TCs during Boreal Summer

It was expected that there would be 10-13 TCs generated in the South China Sea and the Northwest Pacific Ocean in the summer of 2023, close to normal (11); the number of TCs landing on China would be 4-6, close to normal (4.8); the overall strength of typhoon would be medium

to strong; and the typhoon activity path would be mainly northwest, with high possibility of northward heavy impact TCs.

In fact, it showed that 10 TCs generated in the Northwest Pacific Ocean in summer of 2023, two of which landed on China. The number of genesis was close to normal and the number of landfall was less than normal. The prediction of typhoon genesis frequency was consistent with the observation. The prediction had a good grasp of the overall intensity trend and prevailing path of typhoons in summer. It was accurately consistent with the northward TC activities highly affecting China. While there was a certain deviation between the prediction and observation on the landing number of TCs in summer. However, on the view of services, it provided enough warnings to the government and the local people. Two TCs landed in July. Among the TCs generated in August, there was one landing on Liaoning province with the intensity of tropical depression in mid-August and two landing on Guangdong province and Taiwan, respectively, in early September.

1.2 Socio-Economic Assessment

By October 23, 2023, total 6 TCs had affected China in this year. Loss statistics caused by these TCs read as follows, affected population of 9.67 million people in 8 provinces (autonomous regions), 9 deaths and missing persons, evacuated population of 2.36 million people and relocated population of 768,000 people; collapsed housing of over 5100 rooms and damaged housing of over 34,000 rooms; affected crops of 345,500 hectares and destroyed crops of 28,400 hectares. Among all disaster-affected regions, Fujian and Guangdong suffered more impact. In 2023, TCs that affected China demonstrated four characteristics. First, number of TCs was relatively less. Total 16 TCs were generated in northwest Pacific Ocean and south China Sea, and 5 of them made landfalls in mainland China, which were less than usual years. Besides, a tropical depression made landfall. Second, intensity of TCs was stronger. Three out of five TCs, that are, Doksuri (2305), Saola (2309), and Haikui (2311), made their landfalls at strong typhoon levels. Third, landing sites were concentrated, mainly in Guangdong and Fujian. Fourth, losses were heavy in local regions. Typhoon Doksuri caused serious losses in Fujian. Several cities in the Guangdong-Hong Kong-Macao Greater Bay area suffered severe urban waterlogging, due to heavy rainfall brought by the remnant cloud system of Typhoon Haikui.

On July 28, Typhoon Doksuri (2305) made landfall in Jinjiang County, Fujian Province with strong typhoon level. It was the second strongest TC that made landfall in Fujian since 1949, whose intensity was only lower than Typhoon Moranti (1614) in 2016. Doksuri caused severe urban waterlogging and flash floods in Fujian and Zhejiang, as well as heavy impact to tourism, traffic, power supply, and agriculture. In addition, the residual cloud system of Doksuri went north and caused great losses in north China. Total 2.95 million people were affected, 492,000 people were evacuated, and 264,000 people were relocated. In September, TCs Saola and Haikui successively made landfalls. On September 2, Typhoon Saola (2309) made landfall in Zhuhai City, Guangdong Province, with strong typhoon level. It was the second strongest TC that made landfall in the Pearl River Delta region on record, which was only after Typhoon Hato (1713) and demonstrated characteristics of strong intensity and long duration at super typhoon level. On September 3, Typhoon Haikui (2311) made three landfalls in China, and its residual cloud system continuously hovered along the southeast coast of China. From September 3 to 14, sustained heavy rainfall occurred in Fujian and Guangdong. The process intensity of rainfall in Fujian was the second strongest since 2005, only after Typhoon Bilis (0604). The process intensity of rainfall in Guangdong was the second strongest since 2003. Typhoon Haikui demonstrated

characteristics of high rainfall intensity and extreme precipitation, which resulted 26 rivers in Fujian and Guangdong exceeding alarm water levels. Several cities suffered geological disasters, urban waterlogging, and serious infrastructure damage.

Among those landfall TCs, Duksuri (2305) and Haikui (2311) had brought ongoing disasters even aftern their downgrade to TD as remnants on land.

Table 1 Statistics of TCs landfalls and losses in China.

Name & Number	Information of landfall (Time(UTC)/ Location/ Intensity)	Affected provinces	Affected population (10,000 persons)	Dead and missing population (person)	Population of emergency evacuation (10,000 persons)	Evacuated and relocated population (10,000 persons)
Talim (2304)	17th July 14:20 /Zhanjiang, Guangdong/TY 17th July 21:45/Beihai, Guangxi/STS	Guangdong, Guangxi, Hainan	91.7	0	20.3	4.3
Doksuri (2305)	28th July 01:55/Jinjiang, Fujian/STY	Zhejiang, Anhui, Fujian, Jiangxi, Guangdong	295	0	49.2	26.3
Khanun (2306)	11th August 15:00/Zhuanghe, Liaoning/TD	Heilongjiang	4.3	0	1.7	6.5
Saola (2309)	1st September 19:30/Zhuhai, Guangdong/STY 2nd September 05:50/Hailing, Guangdong/STS	Fujian, Guangdong, Guangxi, Hainan	228.1	2	117.1	25.3

Name & Number	Information of landfall (Time(UTC)/ Location/ Intensity)	Affected provinces	Affected population (10,000 persons)	Dead and missing population (person)	Population of emergency evacuation (10,000 persons)	Evacuated and relocated population (10,000 persons)
Haikui (2311)	3rd September 07:30/Taidong Taiwan/STY 4th September 21:20/Dongshan Fujian/TS 4th September 22:45/Raoping Guangdong/TS	Fujian, Jiangxi, Guangdong,	312	6	43.5	17.7
Koinu (2314)	5th October 00:20/Pingdong Taiwan/STY	Guangdong, Hainan	9.1	0	6.8	0.3
Sanba (2316)	19th October 00:00/Dongfang Hainan/TS 20th October 01:45/Suixi Guangdong/TS 20th October 11:40/Lin'gao Hainan/TD	Guangdong, Guangxi, Hainan	213.2	4	7.6	2.1
total			1149.1	12	244.6	76.1

1.3 Regional Cooperation Assessment

1.3.1 The Senior Management and Operation Courses on Tropical Cyclone Monitoring and Forecasting of CMA

The Senior Management and Operation Courses on Tropical Cyclone Monitoring and Forecasting will be organized by CMA Guangdong Meteorological Service and CMA Training Centre (WMO RTC Beijing) in Guangzhou, China from 20th November to 1st December 2023. This program is sponsored by CMA. The course aims to provide knowledge and skills of TC monitoring and forecasting and enhance the trainees' understanding of management of TC disaster risk and disaster prevention mechanism in supporting TC monitoring, forecasting and warning operations. The course will include the interpretation of TC disaster prevention and mitigation mechanisms, the application of artificial intelligence (AI) in TC workflow, the overview of the progress in TC observation experiment, the analysis of TC forecasting and impact assessment. The course will be open to senior management officials (director level and above) and senior meteorologists (meteorologists are expected to have over five years of experience in TC monitoring and forecasting) from national and regional meteorological and hydrological organizations.

1.3.2 Training Course on Hydrological Monitoring and Forecasting Technology for Developing Countries

The project of Training Course on Hydrological Monitoring and Flood Management for Developing Countries from 2023 to 2025, proposed by IC of MWR of China in cooperation with Nanjing Research Institute of Hydrology and Water Conservation Automation (NIHWA), was launched officially at TC 55th Session. It was approved that, as the annual activities/implementation plan for the project, a two-week training course will be held annually with funding support from China government in forms of video, hybrid or face-to-face, depending on the situation of the COVID-19. From Sep 13 to 26, the first training course was held via the internet with 65 participants from 25 countries including Cambodia, Laos, Malaysia, Philippines, Thailand, Vietnam. Dr. Duan Yihong, the Secretariat of Typhoon Committee, Dr. Liu Zhiyu, the Deputy Director of Hydrology Division of the Water Resources Ministry, and Miss Silvana Alcoz from Hydrology and Water Resources Service Office of WMO, delivered welcome speech on the opening ceremony (Fig. 1.12).

Fig. 1.12 Training Course on Hydrological Monitoring and Flood Management for Developing Countries in 2023.

1.3.3 Progress of Tropical Cyclone Research and Review in 2023

Tropical Cyclone Research and Review (TCRR) mainly focuses on topics of tropical cyclone (TC) intensity and structure, TC genesis, TC precipitation, TC climatology, review of TC in history, operational TC forecast verification, TC induced storm surge and flood, and risk management etc. TCRR has published 47 issues since its launch in February 2012 through October 2023. A total of 4 special issues of WMO IWTC are planned to be published in 2023, and a special issue on the 50th anniversary of ESCAPE/WMO PTC is also in preparation.

Quality of the TCRR journal is ensured by strict peer-review, with two-thirds of the reviewers are overseas experts. Authors come from 20 different countries and regions can finish the submission and peer-review through the ScholarOne system of Clarivate Analytics. Currently, TCRR is included in two full-text databases: ScienceDirect and DOAJ, in which

all of the published papers are easily and freely available. TCRR was included in the Emerging Sources Index (ESCI) in 2017, so as a Web of Science Core Collection™ journal, TCRR received its first Journal Impact Factor (JIF)™ of 2.9 in 2023. It was ranked 63 out of 109 (Q3) in the JCR Meteorology & Atmospheric Sciences category. And TCRR was included in Scopus at the end of 2022, so it also received its first CiteScore of 3.4 in 2023. It was ranked in Q2 in three categories (34 out of 103 in Safety Research, 128 out of 316 in Modeling and Simulation, and 30 out of 72 in Computers in Earth Sciences).

II. Summary of Progress in Priorities supporting Key Research Areas

2.1 Application and Evaluation of AI Weather Models in Tropical Cyclone Forecast

Due to the development of the Transformer Model in the field of machine learning, a series of artificial intelligence meteorological large models have emerged since November 2022, such as NVIDIA's FourCastNet and Huawei's Pangu Weather Model. These models have demonstrated performance comparable to or even exceeded traditional numerical weather prediction models on multiple forecast indicators within the short-and-medium-term forecast periods. As a result, they have gained significant attention both within and outside the meteorological departments.

The National Meteorological Centre (NMC) of China Meteorological Administration (CMA) began its collaboration with Huawei at the end of 2022 to utilize the Pangu Weather Model. By the end of July 2023, NMC has successively completed the local deployment and application of 3 artificial intelligence meteorological large models, including "Pangu" (from Huawei), "Fengwu" (from Shanghai Artificial Intelligence Laboratory), and "Fuxi" (from Fudan University). This has led to the real-time operation of these large models. Additionally, NMC has developed a multitude of visualized products and complementary

product display platforms for typhoon forecasting and short-and-medium-term meteorological forecasting. Evaluations of the models' forecasting performance have been conducted from various perspectives, including the forecasting of typhoon intensity and track, atmospheric circulation situation, and meteorological element (Fig.2.1).

Preliminary evaluation results indicate that the AI weather models do not exhibit an absolute advantage compared to traditional numerical weather prediction models, and the error characteristics displayed by different typhoon cases vary. Furthermore, there is a noticeable bias in the forecast of typhoon intensity. From the field verification of circulation situation, the root-mean-square error of mid-troposphere predicted by Pangu model is smaller than that of ECMWF model. However, there is an underestimation of the intensity of key weather systems, leading to more significant deviations in surface and lower-level element forecasting. Comprehensive and detailed evaluations, including retrospective assessments over past several years, are still ongoing (Table. 2.1).

Priority Areas Addressed:

Meteorology

- Enhance the capacity to monitor and forecast typhoon activities particularly in genesis, intensity and structure change.
- Develop and enhance typhoon analysis and forecast techniques from nowcast to medium-range, and seasonal to long-range prediction.

Contact Information:

Member: China

Name of contact for this item: Nie Gaozhen

Telephone: +86-010-58995842

Email: niegaozhen@cma.gov.cn

Name of contact for this item: Zhu Xuesong

Telephone: +86-021-54896126

Email: zhuxs@typhoon.org.cn

2.2 Advances in Numerical Modeling of Tropical Cyclone

2.2.1 Technological Improvement and Performance of CMA-TRAMS

Up to 12th October 2023, the CMA-TRAMS has shown reliable and stable performance for forecasting typhoons as usual. And all 15 typhoons that formed within the model domain were successfully forecasted by CMA-TRAMS. Verification shows that the 24h, 48h and 72h track forecast errors of CMA-TRAMS were 54km, 90.7km, and 141.6km, respectively, and the intensity forecast errors were 10.0hPa, 14.8hPa, and 16.7hPa, respectively (Fig. 2.2). Five typhoons had made landfall in China, namely Talim (2304), Doksuri (2305), Saola (2309), Haikui (2311), and Koinu (2314). In terms of tropical cyclone genesis, CMA-TRAMS forecasted them at least 96 hours in advance. Saola (2309) was the second typhoon made landfall in Guangdong Province with complex track and strong intensity. CMA-TRAMS successfully captured the complex track of Saola (2309), the forecasted tracks matched well with the observed ones throughout all the forecasts with different initial times (Fig. 2.3), In particular, the 24h, 48h, and 72h track forecast errors were 48km, 92km, and 134km, respectively.

2.2.2 Operational Upgraded of Global Numerical Forecast System CMA-GFS V4.0

CMA-GFS upgraded from V3.3 to V4.0 at 00:00UTC on 22th May, 2023, with the horizontal resolution increased from 25km to 12.5km. The model dynamics framework, physical processes, data assimilation technology and data application, as well as the code parallelism were optimized and improved in CMA-GFS V4.0. The improvements in model dynamics and physical processes have significantly improved the model computational efficiency with the computation time saved above 30%, reduced the loss of mass during long-term integration, alleviated the phenomenon of excessive convective precipitation distribution and high proportion of total precipitation, which comprehensively improved the precipitation forecast scores of various magnitudes in East Asia; The improvement of the assimilation framework has increased the accuracy of the tangential linear approximation, improved the timeliness of the four-dimensional variational analysis, and established a 12.5km assimilation analysis system that can be operated stably, with a significant reduction in the analytical errors for each variable and a obviously improvement in the forecasting skill for the first three days. Through technical research, the assimilation application of water vapor channel data of METOP-C AMSUA/MHS/IASI, NOAA-20 ATMS/CrIS, GCOM-W AMSR2, GOES16/17 ABI, H8 AHI, MT1 SEVIRI, and FY4A, have been

successfully used. All of the above instrumental observations have been applied to the CMA-GFS V4.0, with obviously positive contributions to the accuracy improvement of the analyzed fields.

The fast radiative transfer model ARMS developed by CMA has formed a stable and reliable version V1.2.0 in 2023, which has been integrated and operated in CMA-GFS V4.0. The retrospective run shows that after the application of ARMS, the larger scale field forecast of CMA-GFS V4.0 has been improved, the precipitation forecast especially the heavy precipitation forecast is further improved, and the false rate is reduced.

The results of the retrospective run from 31th August, 2021 to 30th August, 2022 show that the average path error and intensity error of CMA-GFS V4.0 are significantly reduced for the entire prediction (Fig. 2.4).

2.2.3 The Development and Operational Test of the 25km Global Ensemble Prediction System

The CMA-GFS V4.0 version is used in the new 25km ensemble forecast system. The ensemble forecast process and corresponding computational module are updated to take into account the differences between the GFS V3.3 and GFS V4.0 versions, and a 25km global ensemble forecast test system based on the GFS V4.0 is established

including the post-processing system. The initial perturbation parameters and model perturbation parameters are the same as those of the operational GEPS. The ensemble prediction test is performed, and the results are analyzed and evaluated in comparison with the operational GEPS ensemble results. The results show that the ensemble average error and dispersion relationship of the 25km ensemble prediction system are reasonable, and also show certain advantages in individual precipitation intensity, distribution and typhoon intensity prediction relative to the operational ensemble prediction.

2.2.4 Optimization of Higher Resolution CMA-TYM

The CMA-TYM adopts a semi-implicit, semi-Lagrangian integration scheme, in which the non-central differential coefficient is an important factor affecting the stability of the model computation as well as the accuracy of the model computation, while the model integration step size directly affects the model stability and the real time for the whole integration. To achieve a better balance among above factors, more experiments are carried out on the basis of the version of CMA-TYM (TYM 4.5km) developed in 2022.

Priority Areas Addressed:

Meteorology

- Enhance the capacity to monitor and forecast typhoon activities particularly in genesis, intensity and structure change.
- Develop and enhance typhoon analysis and forecast technique from short-to long-term.

Contact Information:

Member: China

Name of contact for this item: Ma Suhong

Telephone: +86-010-68400467

Email: mash@cma.gov.cn

Name of contact for this item: Zhang Xubin

Telephone: +86-020-39456428

Email: xbzhang@gd121.cn

2.3 Tropical Cyclone Observation Experiment

2.3.1 TC Field Observation Experiments in 2023

A scientific field experiment on Typhoon Haikui (2311) was successfully conducted by the Shanghai Typhoon Research Institute from 3rd to 6th September, 2023 in Zhangzhou, Fujian Province, China, with the primary focus on typhoon precipitation and structural changes. Multiple observation instruments used include GPS sounding, boundary layer wind profiler, laser raindrop spectrometer, automatic weather station, and those fixed in Zhangzhou station, such as laser wind profiler, micro rain radar, millimeter-wave cloud radar, and 2D raindrop spectrometers. These instruments worked together in a coordinated manner to collect valuable multi-source precipitation data under the strong wind conditions (Fig. 2.5).

2.3.2 Development of an Integrated Ocean Observation Test Platform

An integrated ocean observation test platform (Fig. 2.6) has been developed, which collects seven types of ocean observation data, including global drifting buoys, anchor buoys, ship stations, unmanned boats, offshore platforms, Argo buoys and ice buoys, and covers ocean meteorological and hydrological elements such as sea temperature, wave height, current velocity, air pressure, air temperature, relative humidity, visibility and wind. The quality control algorithm for marine

meteorological and hydrological elements developed independently by the Ocean Observation Technology Innovation Team of the Meteorological Detection Center of the China Meteorological Administration has been incorporated to realize automatic quality control of marine observation data.

In 2023, the oceanographic data provided by the platform provided important support for forecasting the path and intensity of typhoons Doksuri (2305), Saola (2309), Haikui (2311) and Koinu (2314). Especially during Typhoon Saola (2309), the observation data from the research vessel "Zhong Shan Da Xue" was transmitted to the platform in time, which provided the first-hand observation information for the typhoon service.

Priority Areas Addressed:

Meteorology

- Enhance the capacity to monitor and forecast typhoon activities particularly in genesis, intensity and structure change.

Contact Information:

Member: China

Name of contact for this item: Zhu Xuesong

Telephone: +86-021-54896126

Email: zhuxs@typhoon.org.cn

Name of contact for this item: Li Xiaoxia

Telephone: +86-010-58993401

Email: Lxxaoc@cma.gov.cn

2.4 Collaborative Sky Observation of Haiyan I unmanned Aerial Vehicle and BeiDou Navigation Flat Drift

From August to October 2023, under the unified deployment of the China Meteorological Administration(CMA), Meteorological Detection Center of CMA, together with the Hainan Provincial Meteorological Bureau, the Guangzhou Institute of Tropical Marine Meteorology, the Numerical Prediction Center and other units have carried out joint and collaborative observation of high-altitude large unmanned aerial vehicles (UVA) and Beidou flat drift sounding system on the typhoon impact path and target area for typhoons Saola (2309), Haikui (2311) and Koinu (2314). Under the background of multiple typhoons, Petrel I UAV equipped with the dropsonde system has flown 3 sorties with a total flight time of 7hours and a total distance of about 3,200km by 10th October. A total of 28 dropsondes have been dropped and 49,000 effective observation data have been obtained (Fig. 2.7 and 2.8), which have been entered into numerical mode and morning consultation in real time and provided strong support for typhoon forecasting and service. Among them, on 2nd September, the CMA-TRAMS model assimilated the observation data into the forecast experiment, which showed that Typhoon Haikui (2311) tended to move in a more westerly direction after the assimilation, The observation data on 3rd September were evaluated by CMA-TRAMS model and indicated that the landfall intensity of

Typhoon Haikui (2311) was slightly stronger than that of the business, and its path was forecast to have little impact, and it would make landfall at the Fujian-Guangdong border.

Mobile observation data provides direct observation data support for typhoon path prediction and intensity reporting, and has symbolic significance in promoting the construction of mobile observation business for typhoons in the South China Sea, leveraging the benefits of mobile observation for typhoon monitoring and forecasting services, and building the first line of defense for disaster prevention and reduction.

Priority Areas Addressed:

Meteorology

- Enhance the capacity to monitor and forecast typhoon activities particularly in genesis, intensity and structure change.

Contact Information:

Member: China

Name of contact for this item: Ma Suhong

Telephone: +86-010-68400467

Email: mash@cma.gov.cn

Name of contact for this item: Zhang Xubin

Telephone: +86-020-39456428

Email: xbzhang@gd121.cn

Name of contact for this item: Li Xiaoxia

Telephone: +86-010-58993401

Email: Lxxaoc@cma.gov.cn

2.5 Applications of Fengyun Satellites in Tropical Cyclone Operation and Research

2.5.1 Improved Applications of Fengyun Series Satellite Service Platform

Integrate the application of Fengyun Earth service platform to promote the application of FY-4B and FY-3G new generation remote sensing datasets

Since the operation of the "Fengyun Earth Satellite Meteorological Service Platform" developed by the National Satellite Meteorological Center, it has integrated observation data including FY-4B geostationary and FY-3E polar orbit meteorological satellites, giving full play to the different characteristics of satellite channels, using water vapor images to reveal the large-scale background of typhoons such as Super Typhoon Doksuri (2305), Typhoon Saola (2309) and Super Typhoon Haikui (2311), and using true color (visible light) cloud maps to reveal the subtle structural characteristics of typhoon eye walls and peripheral spiral cloud belts. Providing quantitative products such as encrypted observation cloud map with 1-minute and 250m resolution, automatically identification of convective cloud, northwest Pacific Ocean surface wind, atmospheric motion vector, fusion sea surface temperature, and subtropical high products, to serve the whole process of typhoon development and variation. Based on the wind field measurement radar

instrument of the Fengyun-3E, and the precipitation product of the Fengyun-3G, the service for typhoon monitoring and early warning has been carried out. The wind speed inversion of FY-3E WindRAD and the PMR precipitation monitoring results of FY-3G improved the forecast and early warning monitoring capabilities of typhoon, such as Saola (2309) and Haikui (2311). We communicated with the Central Meteorological Observatory, decision-making departments and associated media to understand the demands, take the initiative to dock with the Central Meteorological Observatory and meteorological stations at the coastal provincial such as Shanghai, Zhejiang, Fujian, Guangdong, and Hainan, and timely provide satellite monitoring products with local characteristics.

2.5.2 Operational Applications of FY-3D Micro-Wave Radiation Data

Micro-Wave Radiation Imager-I on FY-3D with the 1400-km width is able to capture Typhoon Doksuri (2305) in the South China Sea before landfalling. The 89GHz channel of the FY-3D microwave imager is very sensitive to precipitation scattering signals, mainly used to obtain ground precipitation information. Typhoon Doksuri was monitored using microwave data from the FY-3D microwave imager, its concentric eyewalls (CE) structure was clearly identified. According to the TC

center information acquired from the bulletin issued by the National Meteorological Center in operational work, cross-sections were made. The moat area had a bright temperature of about 280K, which formed a clear contrast with the low bright temperature of inner and outer eyewalls and enabled the identification of CE.

Based on the synthesis analysis of wind speed from synthetic aperture radar and land-based radar, the diameter of eye, inner eyewall, outer eyewall, as well as the width of moat, could be quantitatively defined using specific thresholds. Techniques under the program FY-APP-2022.0110 support the forecasters in NMC/CMA in analyzing TC structure and intensity before landfall. Contribute to accurate landfall forecasting and disaster prevention and mitigation (Fig. 2.9).

2.5.3 Assimilations of FY-4B AGRI Water Vapor in a Regional-Typhoon Unfiled Model

Chinese Fengyun-4B (FY-4B) is a new-generation high-resolution geostationary satellite, with three water vapor channels equipped on Advanced Gravimetric Remote Imager (AGRI) to detect the water vapor distribution in the upper, middle, and lower layers of the troposphere, respectively. In this study, the FY-4B AGRI data are transferred into the GSI assimilation system and assimilated for the first time. In the meantime, a 60km sparse grid, Variable Variation Bias Correction

Scheme (VarBC), and the observational error of 2.2K are adopted in Shanghai 9km regional-typhoon unfiled model and the GSI data assimilation system. According to the best-track data, absorbing water vapor channels 9-11 of FY-4B AGRI enhances the prediction of Typhoon Doksuri (2305) route after 36hours by around 5% and greatly improves the forecast of its intensity after 36hours (Fig. 2.10).

2.5.4 FY-4B Specialized Observation Experiment for Typhoon KHANUN

In order to monitor the catastrophic weather impacts of Typhoon Khanun(2306) on East and North China, develop and improve the satellite target observation driven by forecasting needs, and improve the assimilation and forecasting accuracy of CMA-GFS, the National Meteorological Center (NMC), the National Satellite Meteorological Center (NSMC) and the CMA Earth System Numerical Modelling Center (CEMC) have jointly carried out a special Intensive observation experiment for Khanun (2306) on FY-4B, and the target area for the observation is 120°E-140°E, 20°N-45°N (Fig. 2.11). The domestic numerical prediction model has provided effective technical support for the real-time study and judgment of the subsequent track and intensity change of Khanun.

Through collaborative efforts, NSMC ensured that the intensive observation data could be transmitted to CEMC at the first time after the data was received, and CEMC simultaneously carried out the parallel test of the GIIRS of FY-4B using a parallel test system with the operational system. The forecast results with the intensive observations were used in the morning consultation for three consecutive days. After the first intensive observation of FY-4B GIIRS was assimilated on August 2, the results suggest that, compared to the results of the operational model, there may be a probability of earlier recurve. Later evaluation show that the recurving time and track forecast from the experiment forecast are closer to that of the Best Track (Fig. 2.12)

2.5.5 Preliminary Study of the Assimilation of FY-4A/GIIRS 3D Inverted Wind Field in CMA-MESO

The high temporal resolution geostationary hyperspectral sounding data can not only provide continuous water vapor and temperature vertical sounding information, but can also invert the wind field information at different altitudes by tracking the water vapor information. The world's first Geostationary Hyperspectral Infrared Sounder (GIIRS) is mounted on the FY-4A satellite, which contains 1650 spectral channels, including 689 temperature and 961 water vapor detection channels. During the development of typhoon, FY-4A/GIIRS can start the target

observation and make high time-frequency observation based on the sensitive area calculated by CMA-GFS. A more direct information of the wind field could be achieved by applying a machine learning algorithm to inverting the GIIRS intensive observation into a three-dimensional wind field (Fig. 2.13). Assimilation studies of the inverted 3D wind field are currently being conducted in CMA-MESO to assess the accuracy of the inverted 3D wind field and the impact on typhoon forecasting.

Priority Areas Addressed:

Meteorology

- Enhance the capacity to monitor and forecast typhoon activities particularly in genesis, intensity and structure change.
- Develop and enhance typhoon analysis and forecast technique from short-to long-term.

Contact Information:

Member: China

Name of contact for this item: Ma Suhong

Telephone: +86-010-68400467

Email: mash@cma.gov.cn

Name of contact for this item: Zhu Xuesong

Telephone: +86-021-54896126

Email: zhuxs@typhoon.org.cn

Name of contact for this item: Song Wanjiao

Telephone: +86-010-58995547

Email: songwj@cma.gov.cn

Name of contact for this item: Nie Gaozhen

Telephone: +86-010-58995842

Email: niegaozhen@cma.gov.cn

2.6 Advances in Tropical Cyclone Scientific Research

2.6.1 Investigation of the Mechanism for Secondary Eyewall Formation

Using WRF-ideal simulation, the study reveals that cloud-radiation feedback (CRF) facilitates SEF of tropical cyclones by promoting the formation of outer rainbands (ORBs) and their stratiform sectors. CRF engenders an upper-level anomalous radiative warming in the outer-core region, which induces a secondary circulation that accelerates the release of microphysical heating above the freezing level. The enhanced upper-level latent heating further promotes the outer-core convection and the top-down development of the ORBs. Moreover, CRF promotes a broader stratiform precipitation area and stronger stratiform heating profiles of the ORBs, which forces convective updrafts at the radially inward edge of the stratiform precipitation area and eventually leads to SEF. On the contrary, when the anomalous radiative warming is removed, the organization of ORBs and the development of stratiform precipitation are suppressed due to the absence of the radiation-induced upper-level secondary circulation, thus inhibiting SEF.

Based on multi-source observational and reanalysis datasets, two secondary eyewall formation (SEF) cycles occurring during Super Typhoon Hinnamnor's (2211) lifetime are analyzed. The first SEF happened near the time when Hinnamnor achieved its maximum

intensity, and it seems that its internal dynamics dominated the SEF process after the development of shear-induced asymmetric spiral rainbands. The merger of a tropical depression with Hinnamnor led to a continuous increase in both its inner-core size and outer-core circulation, causing generation of the second SEF. It is inferred that the external and internal dynamics worked together during the second SEF process. The concentric eyewall structure maintained for approximately 84h under the moderate vertical wind shear. Also, unique changes in intensity accompanied the two structural changes (Fig. 2.14).

2.6.2 Driving Forces of Extreme Updrafts Associated with Convective Bursts in the Eyewall of a Simulated TC

Many studies have indicated that convective bursts (CBs) are closely related to TC intensification, but few studies have been conducted on the mechanisms that control the formation and evolution of CBs. In this study, the 1-min output data of a simulated TC are used to understand the convective extreme updrafts of CBs in the TC eyewall. The simulated convective extreme updrafts in the TC eyewall exhibit two peaks at middle and upper levels, respectively, since the effect of hydrometeor loading decelerates the air parcels between the updraft maxima. While the positive buoyancy makes air parcels in the CBs accelerate at middle levels, in agreement with previous studies, it is found that, at the upper

levels, both the positive buoyancy and the upward vertical perturbation pressure gradient force accelerate the air parcels. This study suggests that the vertical perturbation pressure gradient force also plays an important role in the formation of CBs in the TC eyewall (Fig. 2.15).

2.6.3 Suitability Test and Improvement of Thompson Microphysics Scheme

Based on the GRIST model, the simulated precipitation features of Typhoon Lekima (1909) from numerical experiments using different microphysical schemes (WSM6 scheme (noted as WSM6), original Thompson scheme (noted as THOM) and modified Thompson scheme (noted as THOM_NEW) are compared. All the experiments can reasonably reproduce the track of Typhoon Lekima (Fig. 2.16), but the simulated intensities are consistently weaker than the observation (Fig. 2.17). Due to the similar tracks among the simulations and observation, the spatial distributions of accumulated precipitation during the period before and after the landfall of Lekima are consistent with the rain gauge data. However, the simulated precipitation in WSM6 scheme is heavier than the observation mainly caused by that the area of accumulated precipitation that exceeds 150mm is larger. The parameterizations of raindrop size distribution (RSD), the falling velocity as well as the collisional coalescence-breakup process of raindrops in the Thompson

scheme are modified by introducing the multiscale wind information. And finally both the simulated precipitation and RSD by using the THOM_NEW are more comparable with the observation (Fig. 2.18).

2.6.4 Preliminary Analysis on Ensemble Disturbances in Typhoon Track Forecast

Shanghai Weather And Risk Model System-Ensemble Prediction System (SWARMS-EN) gives the accurate typhoon landfall information for 5 days ahead the landfall of Typhoon Muifa (2211). Through the analysis of the ensemble members, it is found that the differences in the large-scale circulation fields are mainly response for the difference in track forecasts. Disturbances in the wind and the temperature in the dynamic unstable region near TC center have the characteristics of flow-dependence. Small disturbances are located in the whole troposphere in the initial field of the simulation, and they develop and spread with the increase of forecast time. The disturbance in the lower troposphere is dominated by disturbance internal energy, while in the upper level disturbance kinetic energy becomes the main component, and plays a leading role in the evolution process (Fig. 2.19).

2.6.5 Research on Extreme TC Precipitation in Eastern China

Analysis of rainfall data from the Tropical Cyclone Yearbook show that Typhoon In-Fa (2106) not only induces record-breaking rainfall accumulations at individual surface stations, but also causes unprecedent rainfall amounts for the whole area of eastern China. Quantitatively, 2, 4, 11, 24 and 55 stations are exposed to once in 200-, 100-, 50-, 20- and 10-year extreme TC rainfall accumulations, respectively, and the accumulative rainfall of 75 stations have break record since 1980. Overall, the return period is up to ~481 years for the total rainfall amount accumulated in eastern China during the 1980-2019 baseline. The extremely long rainfall duration is identified as key to the torrential rains in the Yangtze River Delta before In-Fa changes its direction of movement from northwestward to northeastward, while the extreme hourly rain rate plays a dominant role in the north of Yangtze River afterwards. Probabilities of occurrence of such an unprecedented TC rainfall event have increased in most (~75%) of the eastern China during the period of 2000-2019 compared with those during 1980-1999. Our study highlights the likely increase in risk of extreme TC-induced rainfall accumulations which should be considered in disaster risk mitigation (Fig. 2.20).

2.6.6 Characteristics of Ahead-of-eye-center Cooling in SST for TCs

The characteristics of in-storm cooling occurred ahead-of-eye-center are investigated based on a combination of observations and numerical simulations, as well as its sensitivity to tropical cyclone (TC) characteristics and oceanic climatological conditions. A composite of drifter and remote sensing observations of TC-ocean interaction events from 1979 to 2020 in the North Hemisphere statistically evidences that the percentage of TC-induced ahead-of-eye-center cooling is enhanced remarkably over the coastal ocean than that over the open sea, no matter what the TC intensity, translation speed, TC wind radii and pre-storm SST conditions are. Idealized numerical simulation results show that as the TC center approaches the coastline, the percentage of ahead-of-eye-center cooling increases steadily with the water depth shallowing below 100 meters. This phenomenon may not be caused by strong stratification of the coastal ocean, as previous studies suggested. An ocean heat balance analysis reveals a new mechanism responsible for the enhanced ahead-of-eye-center cooling near the coast: the vertical mixing dominates in the surface cooling process over the open sea, broad while the intense advection is largely responsible for the rapid increase of ahead-of-eye-center cooling over the coastal ocean and induce less cold-water entrainment from below. A series of sensitivity experiments are conducted by varying TC characteristics in terms of intensity, translation speed,

radius of maximum wind speed, and ocean characteristics in terms of temperature profiles and slope rates of the shelf. The percentage of ahead-of-eye-center cooling is dependent on the intensity and translation speed of TCs, but showing little sensitivity to other parameters (Fig. 2.21).

Priority Areas Addressed:

Meteorology

- Enhance the capacity to monitor and forecast typhoon activities particularly in genesis, intensity and structure change.
- Develop and enhance typhoon analysis and forecast technique from short-to long-term.

Contact Information:

Member: China

Name of contact for this item: Zhu Xuesong

Telephone: +86-021-54896126

Email: zhuxs@typhoon.org.cn

Name of contact for this item: Li Ying

Telephone: +86-010-58995830

Email: yli@cma.gov.cn

2.7 Improvement of Typhoon-related Disaster Management

2.7.1 Analysis of Natural Disasters, Meteorological Disasters, and Typhoon Disasters Affecting China from 1989 to 2021

Using data from China Disaster Reduction Network, Yearbook of Tropical Cyclone, China Climate Bulletin, and Statistical Yearbook of China Civil Affairs, statistics are conducted on natural disasters, meteorological disasters, and typhoon disasters in China from 1989 to 2021. It is found that meteorological disasters are the most harmful to people, economy, and crops among natural disasters in China, and typhoon disasters also account for a high proportion of meteorological disasters. Over the past 33 years, although the number of tropical cyclones that have landed in China has not shown a significant linear trend, the number of tropical cyclones that have caused disasters has increased. The proportion of deaths and missing persons, house collapses, affected areas of crops, and direct economic losses caused by typhoon disasters to the gross domestic product has shown a downward trend. This fully demonstrates that the Party Central Committee attaches great importance to disaster prevention, reduction, and relief work, and China's disaster prevention and reduction capabilities have significantly improved. In the past decade from 2012 to 2021, except for the basically stable trend of the affected area of crops, all other indicators have decreased through significance testing. Strengthening modern agricultural

meteorological services will be the focus of improving the typhoon disaster prevention system in the future (Fig. 2.22).

2.7.2 Changes in TC Disasters over China during 2001-2020

TC disasters in China during 2001-2020 were analyzed to reveal their spatial and temporal characteristics from the Yearbook of Meteorological Disasters in China. Furthermore, the impact factors, including TC track, precipitation, and intensity, were further investigated to demonstrate the reasons for decadal changes. During 2001–2020, 274 impact tropical cyclones (ITCs)from the Northwest Pacific Ocean and the South China Sea brought precipitation to mainland China. The frequency of ITCs varied little from year to year, but the TC disaster losses varied broadly. The annual mean affected crop area caused by ITCs in China was 2.1 million ha, and the annual mean affected population was 32.2 million people. The annual mean direct economic loss (DEL) was 62.9 billion RMB, with a significant decreasing trend in the ratio of DEL to GDP. Compared to 2001-2010, the area over China impacted by ITCs expanded during 2011-2020. The frequency of TC disasters increased significantly in Northeast China, Shandong and Yunnan province, while decreased significantly in Hubei province. There has been an increase in TC disasters losses in Yunnan, Guizhou, and North China in the past decade, whereas a reduction has been observed in southeastern China. In

other words, in the past decade, TC disasters have been aggravated in areas relatively less affected by TCs but alleviated in areas heavily impacted by TCs. Increasing frequency, onshore duration, distance travelled, and TC precipitation together contributed to the increase in TC disaster losses in Northern China. (Fig. 2.23).

Priority Areas Addressed:

Integrated

- Enhance activities to develop impact-based forecasts and risk-based warning.

DRR

- Provide reliable statistics of mortality and direct disaster economic loss caused by typhoon-related disasters for monitoring the targets of the Typhoon Committee.
- Evaluate socio-economic benefits of disaster risk reduction for typhoon-related disasters.

Contact Information:

Member: China

Name of contact for this item: Zhu Xuesong

Telephone: +86-021-54896126

Email: zhuxs@typhoon.org.cn

Name of contact for this item: Zhang Daquan

Telephone: +86-010-58995035

Email: zhangdq@cma.gov.cn

2.8 Tropical Cyclone Operational Skill Training of CMA

2.8.1 Training Workshop on Forecasting of Marine Weather

In April 2023, Training Workshop on New Techniques of Marine Meteorological Forecasting was held at the Training Center of CMA in Beijing. This workshop is the first special training workshop focusing on Marine Meteorological Forecasting in recent years, which has been widely concerned and welcomed by forecasters in coastal areas. The 35 trainees were all forecasters from coastal areas or areas seriously affected by typhoon disasters.

The contents of this Workshop contain operational progress in typhoon forecast, dynamic mechanisms related with typhoon genesis and evolutions, new technology and methods of typhoon forecast, typical cases about typhoon forecast and warning service, etc. During the training courses, a variety of training methods were used, such as teaching, practice, communication and discussions. The training lasted for three weeks, including one week of online training. After training, the trainees' operational capabilities of multi-source data were improved, meanwhile, more practical forecast and service concepts and ideas were provided.

2.8.2 Training Workshop on the Applications of Typhoon Numerical Forecast Products

The Training Workshop on the applications of typhoon numerical forecast products has been held in October 2023 in China Training Center with its 39 participants who are the forecasters coming from prefectural and above meteorological services around the coastal provinces in China.

In terms of typhoon the training content mainly covers the issues about basic knowledge of numerical prediction, the theory of typhoon monitoring and forecasting, and application of numerical models in typhoon forecasting etc. The training workshop, through course explanation and practice training, employs comprehensively various training methods such as teaching, practice, communication and discussion in order for familiarizing the forecaster with the operational numerical forecast system and the explanation method of model products in typhoon forecasting, understanding the novel typhoon objective forecast technology, comprehending the principle of typhoon generation and enhancement, mastering the typhoon satellite monitoring method and positioning and strength-determining technology, as well as understanding the application of tropical cyclone data in the Northwest Pacific Ocean so as to improve the ability to apply forecast products in case the forecasters make typhoon prediction.

Priority Areas Addressed:

Meteorology

- Enhance and provide typhoon forecast guidance based on NWP including ensembles and weather radar related products, such as QPE/QPF.
- Enhance, in cooperation with TRCG, training activities in accordance with Typhoon Committee forecast competency, knowledge sharing, exchange of latest development and new techniques.

Contact Information:

Member: China

Name of contact for this item: Zhang Lina

Telephone: +86-010-68409210

Email: zhangln@cma.gov.cn

Annexes

Tab. 2.1. Averaged subjective and objective prediction errors of Typhoon DOKSURI (2305).

	name	24h		48h		72h		96h		120h	
		sample	errors /km	sample	errors /km	sample	errors /km	sample	errors /km	sample	errors /km
Subjective	CMA	26	51.8	22	94.0	18	153.5	14	262.8	10	339.9
	JMA		38.9		80.1		150.6		243.4		324.9
	JTWC		61.0		95.2		167.7		256.6		339.2
Global numerical models and AI	CMA-GFS	28	61.6	24	55.7	20	93.6	8	205.3	6	422.6
	NCEP-GFS		54.2		131.2	20	249.3		411.9		568.1
	ECMWF-IFS		51.3		65.2	20	84.8		118.5		264.3
	Japan		50.9		92.2	20	173.7		308.8		357.1
	Fengwu		42.4		77.4	20	133.5		126.4		127.7
Regional models	Shanghai-TC	12	57.6	10	83.4	8	146.7	/	/	/	/
	CMA-TRAMS		52.7		56.9		117.3		/		/
	HWRF		82.4		180.2		301.6		/		/
	Shanghai-multi model ensemble		38.5		68.7		119.0		/		/

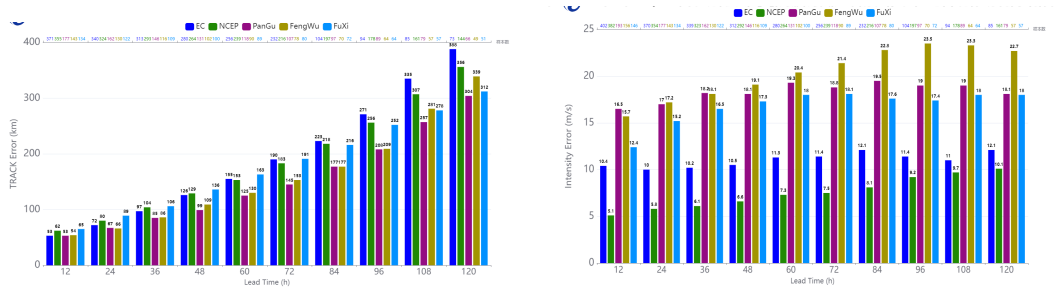

Fig. 2.1 Verifications of numerical and AI meteorological models for TCs in 2023, track errors (left) and intensity errors(right).

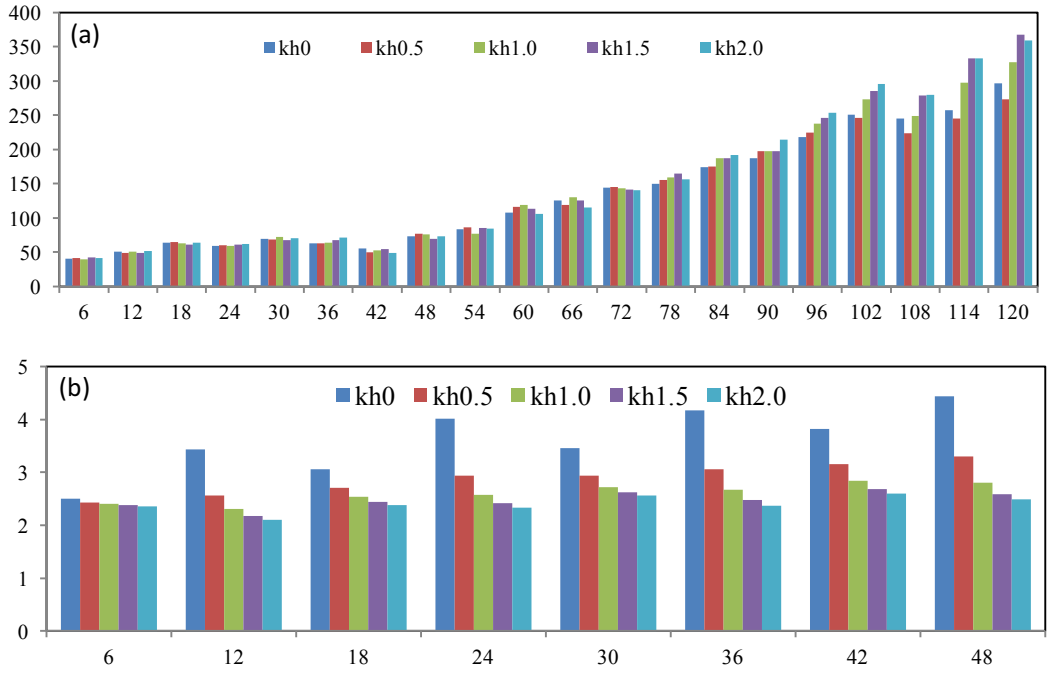

Fig. 2.2 8 typhoon cases under different fundamental diffusion coefficients. (a) average track errors within 120 hours, (b) the RMSE of 2-m temperature within 48 hours.

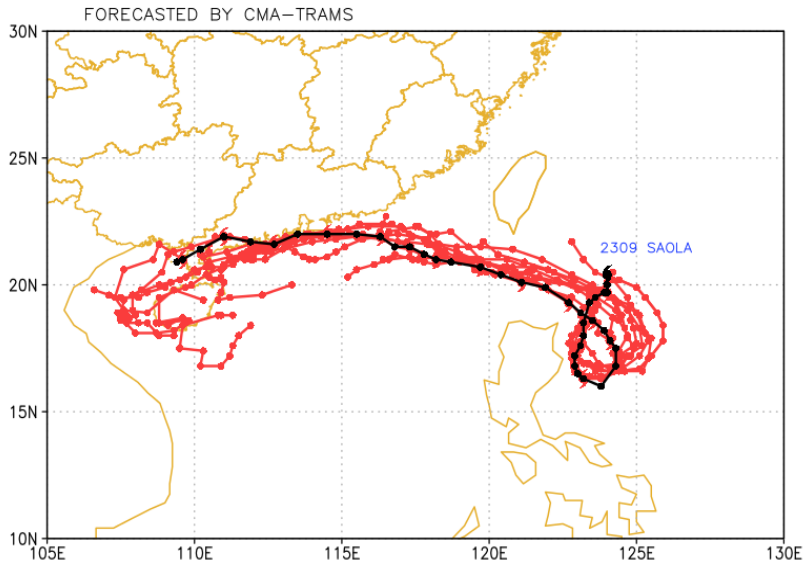

Fig. 2.3 The CMA-TRAMS forecast tracks for Saola (2309) with different initial times (red) in comparison with the observed track (black).

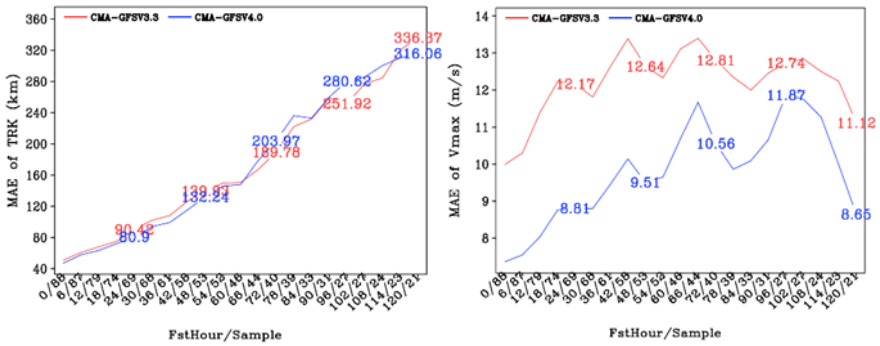

Fig. 2.4 Mean track and intensity errors for retrospective runs of CMA-GFS V3.3 and CMA-GFS V4.0.

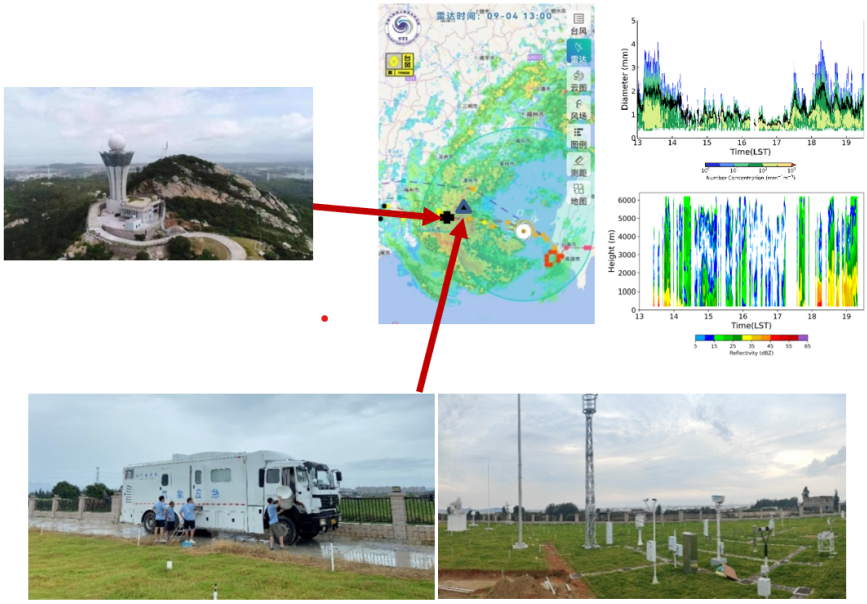

Fig. 2.5 The joint observation experiment of Typhoon Haikui (2311) conducted by the Shanghai Typhoon Institute in the field of the National Meteorological Observation Special Experiment in Zhangzhou.

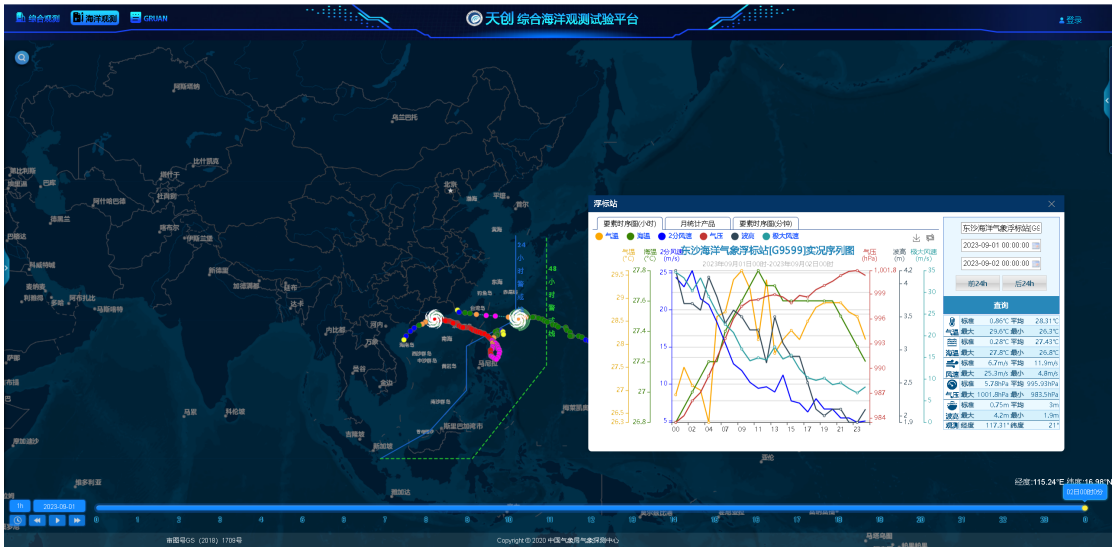

Fig. 2.6 Integrated marine observation test platform.

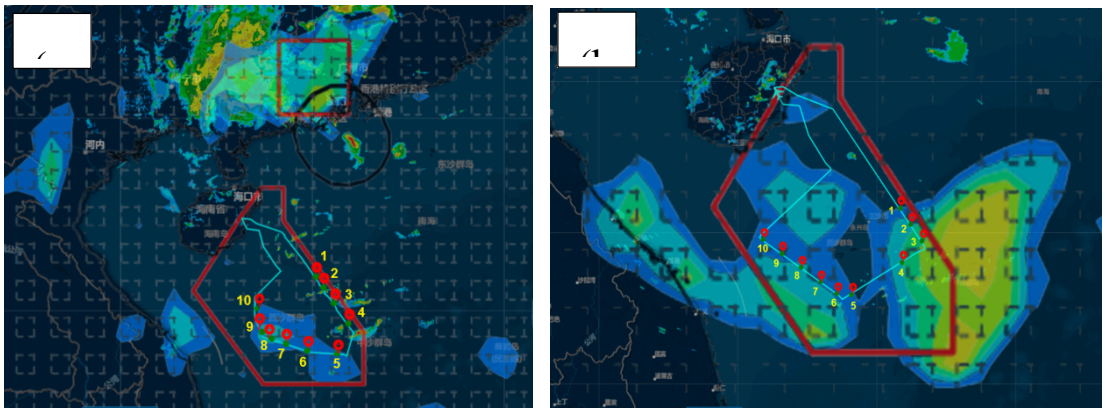

Fig. 2.7 Flight path, drop point and typhoon sensitive area of Petrel I UAV at 21:00(BJT) on September 2 (left) and 18:00(BJT) on September 3 (right).

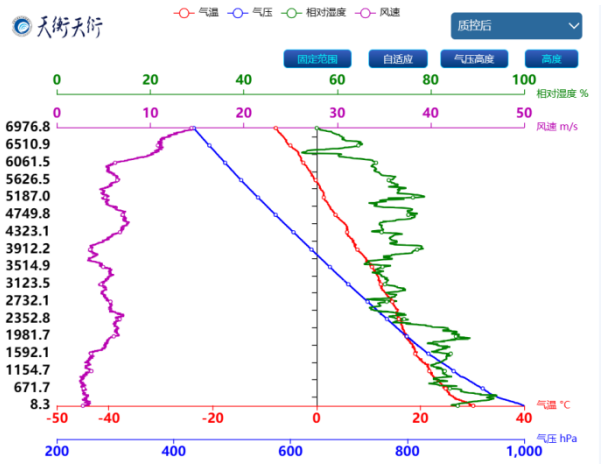

Fig. 2.8 Profile of drop probe at 19:23(BJT) at September 3.

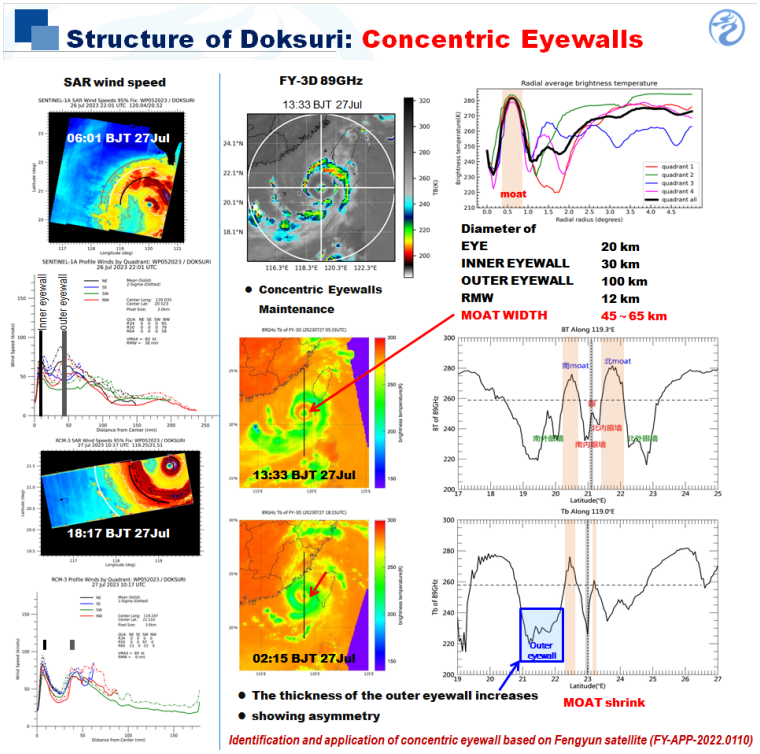

Fig. 2.9 Operational applications of FY-3D Microwave Radiation in Typhoon Doksuri (2305).

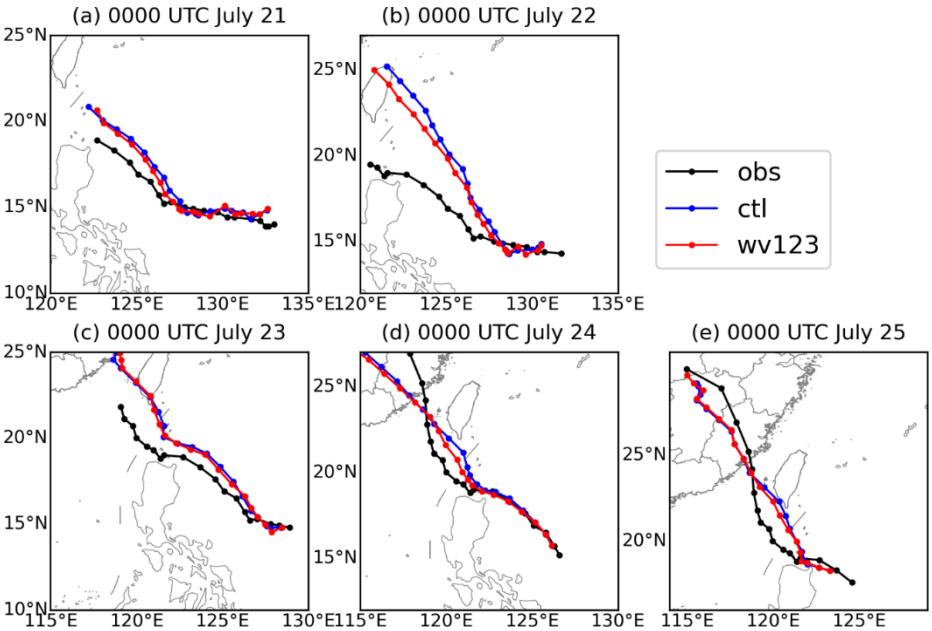

Fig. 2.10 Observed track (black) and 120-hour track forecasts for Typhoon Doksuri (2305) from the CTL (blue) and WV123 (red) experiments starting at 0000 UTC from 21 to 25 July 2023.

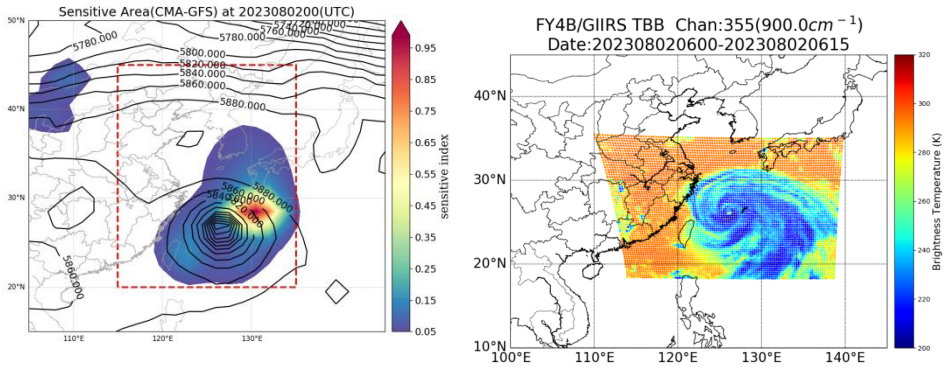

Fig. 2.11 The sensitive area of Typhoon Khanun (2306) and schematic diagram of the bright temperature observation.

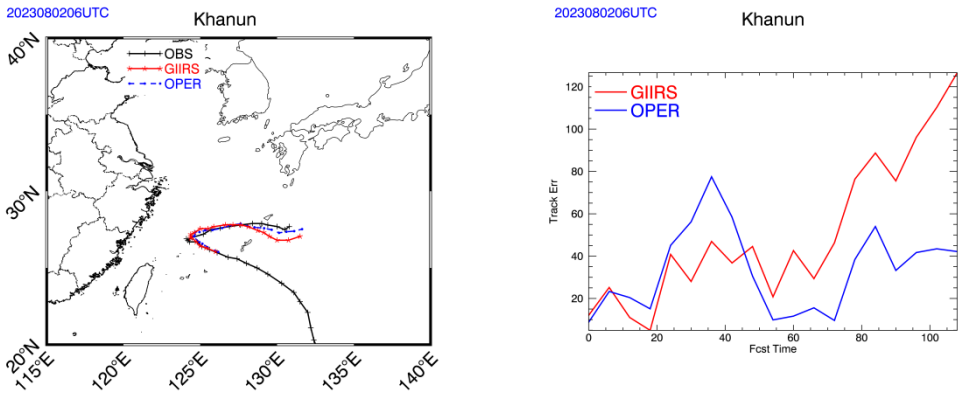

Fig. 2.12 Comparison of intensive observation experiment and operational results for Typhoon Khanun (2306).

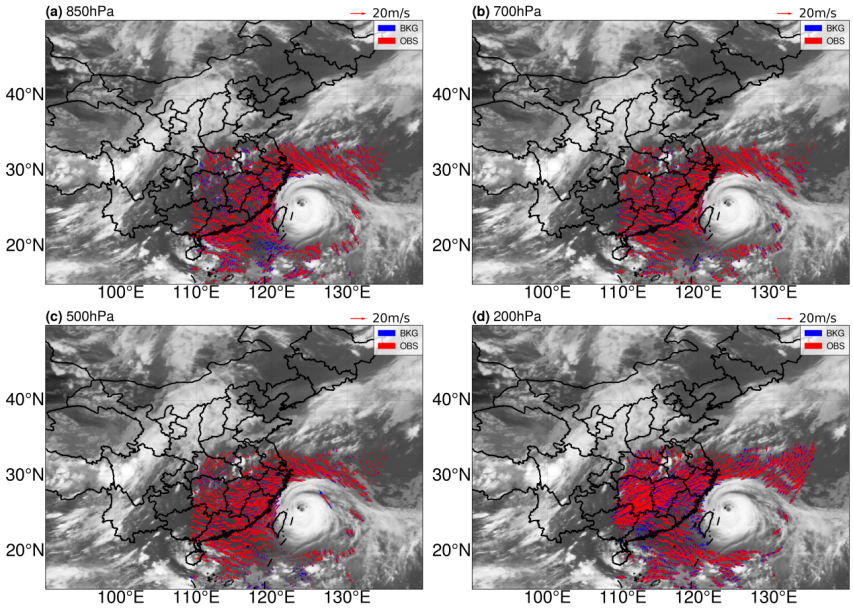

Fig. 2.13 Distribution of 3D inverse wind field (OBS) at different heights (850, 700, 500, 200hPa) during Typhoon Maria (1808) in 2018.

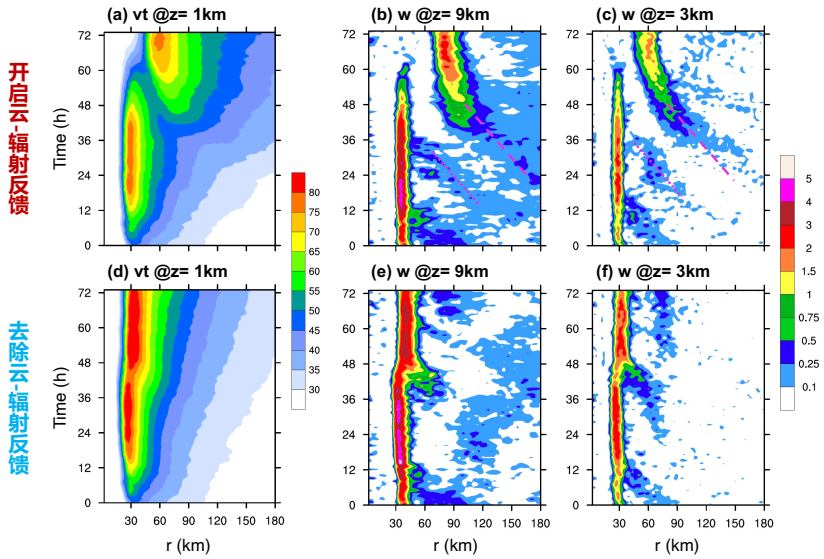

Fig. 2.14 Hovmöller diagram of azimuthal-mean (a) tangential velocity (m/s^1) at z=1km, (b) vertical velocity (m/s^1) at z=9km and (c) vertical velocity (m/s^1) at z=3km for control experiment (CTRL). (d–f) as (a–c), but for NRAD48. The two of magenta lines mark inner rainbands (thin dotted) and outer rainbands (thick dashed) in CTRL.

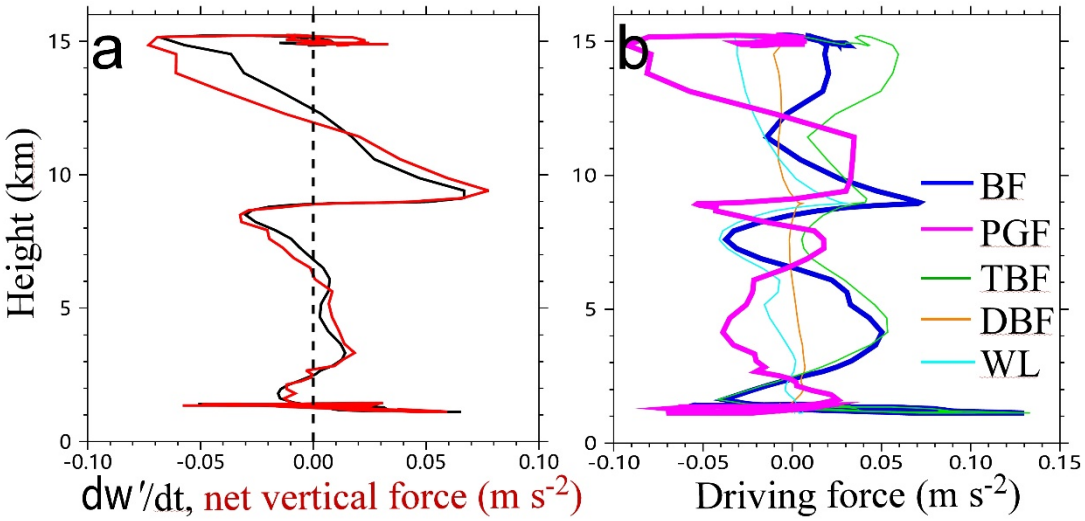

Fig. 2.15 Vertical profiles of (a) the vertical acceleration of perturbations (dw'/dt, black lines, m/s^2) and the net vertical force (red lines, m/s^2), and (b) the buoyancy force (BF, thick blue lines, m/s^2), the vertical perturbation pressure gradient force (PGF, thick magenta lines, m/s^2), the thermal buoyancy force (TBF, thin green lines, m/s^2), the dynamic buoyancy force (DBF, thin orange lines, m/s^2) and the water loading (WL, thin cyan lines, m/s^2).

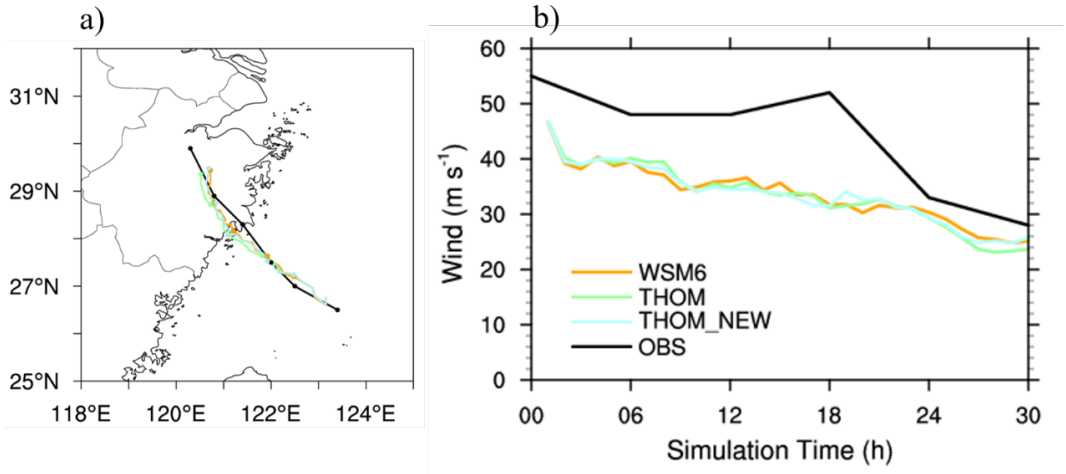

Fig. 2.16 The observed and simulated track and intensity of Typhoon Lekima (1909).

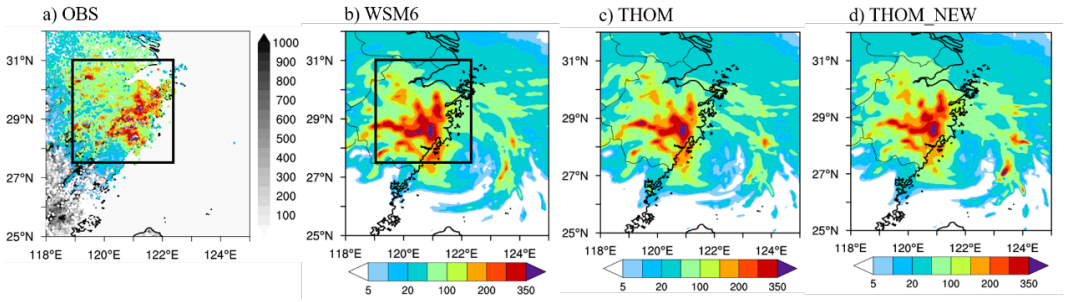

Fig. 2.17 The (a) observed and (b-d) simulated accumulated precipitation from 18:00UTC August 9th to 06:00UTC August 10th. The black square in (a) represents the target area of precipitation.

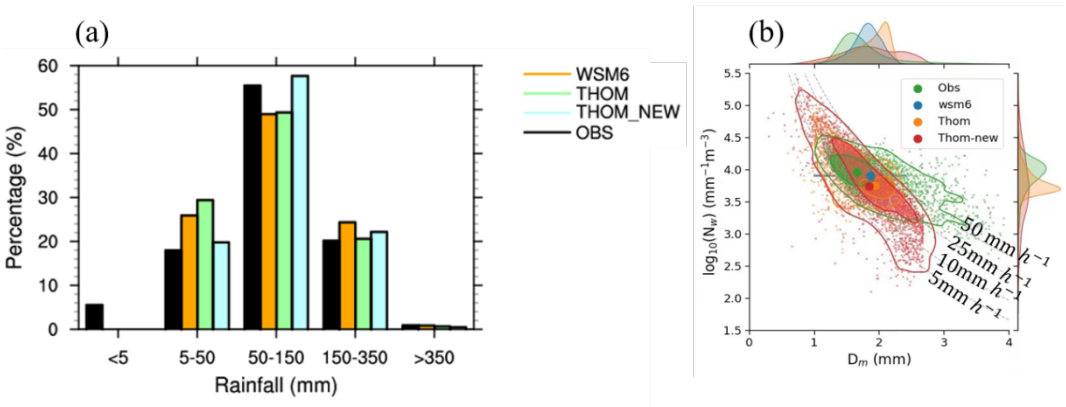

Fig. 2.18 (a) The frequency of different intensity of precipitation within the target area in Figure Xa. (b) The joint probability distribution and scatterplot of D_m(mm) and N_w($mm^{-1}m^{-3}$) within the target area in Figure Xa. Contours are percentages at 25% and 50% with shaded above 50%. The grey dash lines represent the rain rate at 5, 10, 25, 50mm·h^{-1}, respectively.

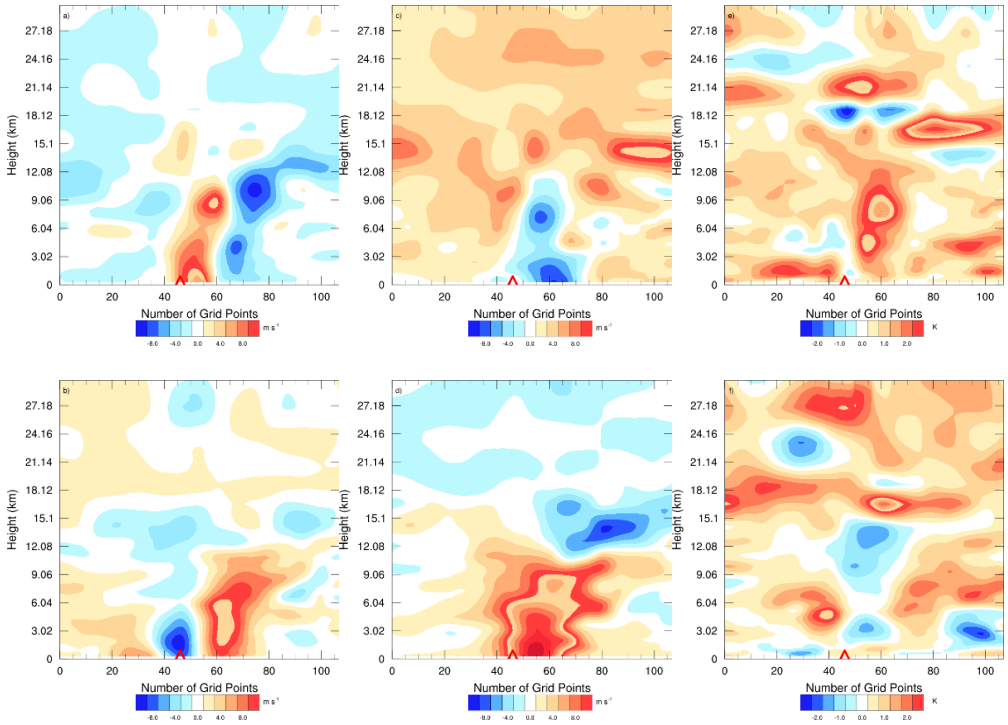

Fig. 2.19 Vertical distribution of horizontal winds and temperature perturbations for ensemble members (a)(c)(e) 7 and (b)(d)(f) 13.

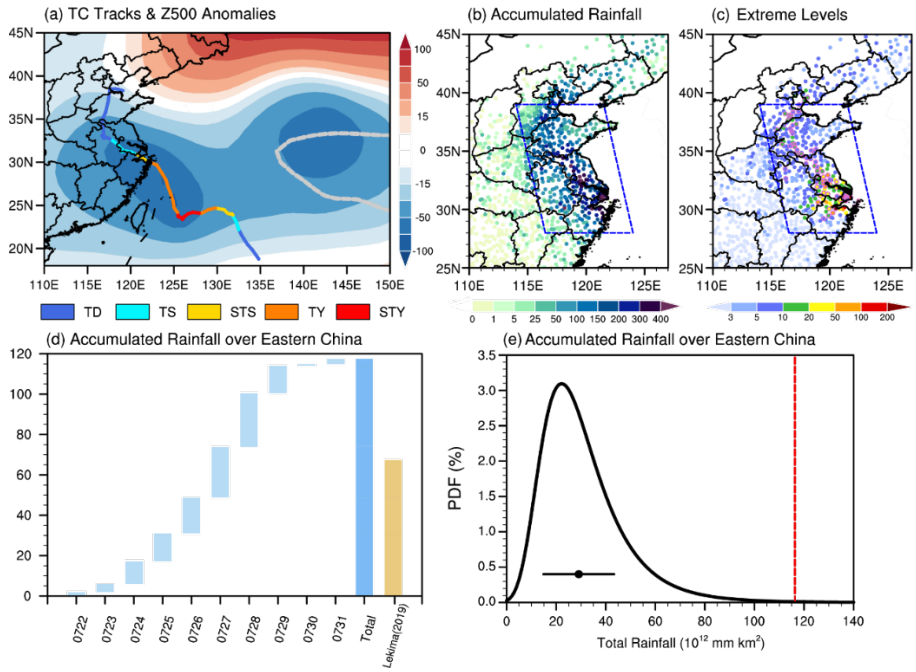

Fig. 2.20 (a) Observed 6-hourly track of Typhoon In-Fa (2106) from 12:00 UTC 16th to 00:00 UTC 31st July 2021. Intensity changes are shown with different colors (dark blue, blue, yellow, orange and red denote tropical depression, tropical storm, strong tropical storm, typhoon and strong typhoon, respectively). Shadings denote the JRA55 background 500hPa geopotential height anomalies (units: m) during the 22nd-31st July 2021, relative to the 1980-2019 climatological mean. Grey dashed line denotes the climatological WNP subtropical high. (b) Accumulated rainfall produced by In-Fa at surface stations from 22nd to 31st July 2021 (units: mm). (c) Return periods of In-Fa's accumulated

rainfall at each station. Light blue, slate blue, green, yellow, orange, red and dark red dots denote stations exceeding the 3-, 5-, 10-, 20-, 50-, 100- and 200-year return values, respectively. Orchid circles denote stations exceeding local maximum values in 1980-2019. (d) Accumulated daily rainfall amount summed over eastern China during 22nd-31st July 2021 (units: mm). Brown bar denotes the total rainfall accumulation in eastern China induced by Typhoon Lekima (1909). (e) Probability distribution function (PDF; units: %) of annual maximum rainfall accumulations over eastern China during 1980-2019.

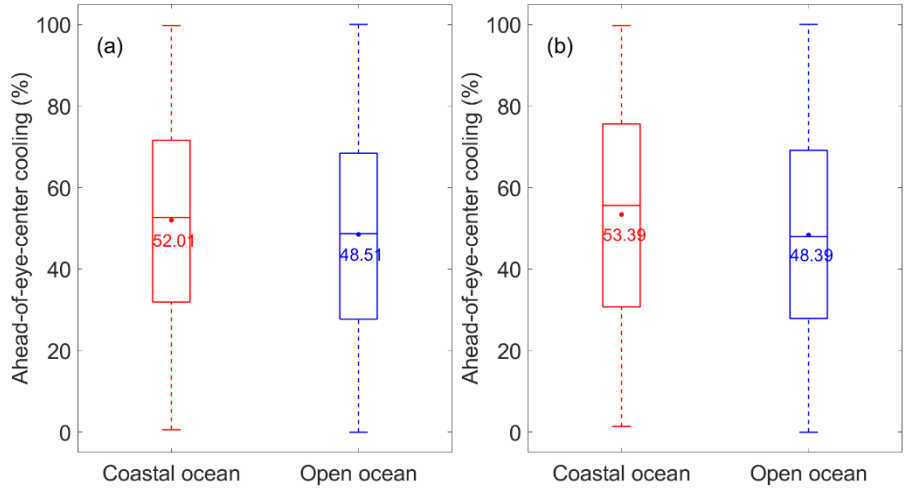

Fig. 2.21 Box and whisker plots of percentages (%) of in-storm cooling occurred ahead-of-eye-center over coastal ocean (red) and open ocean (blue) for (a) land distance classifications and (b) water depth classifications. The small dots and the numerals denote the averaged values.

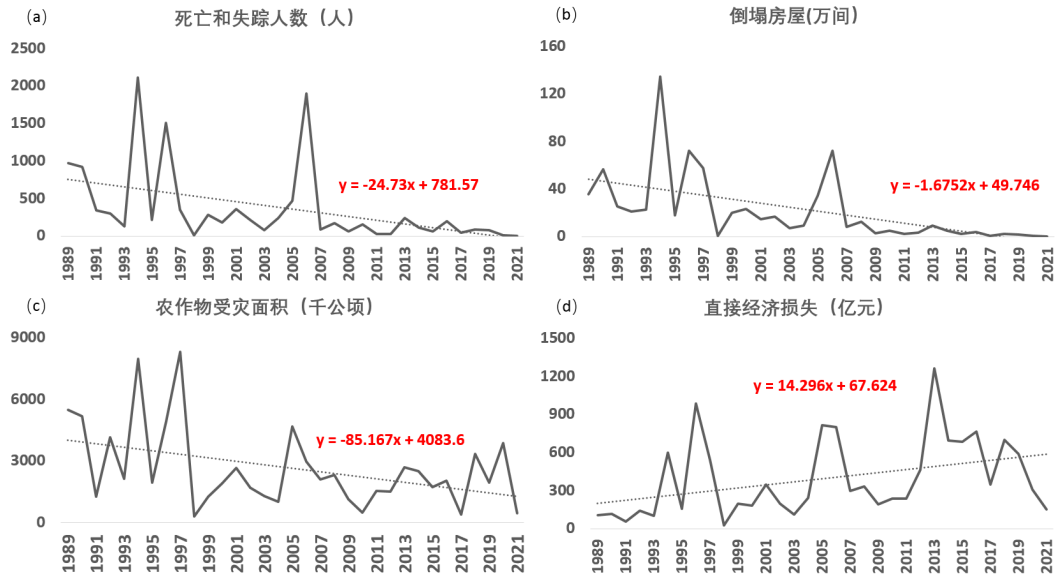

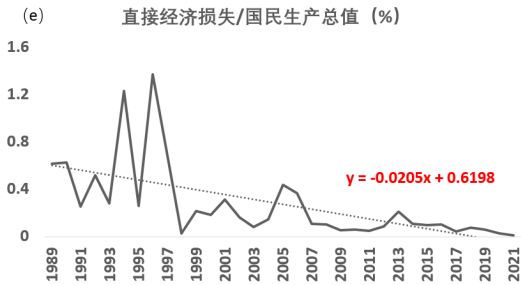

Fig. 2.22 Deaths and missing persons (a), collapsed houses (10000) (b), affected area of crops (1000 hectares) (c), direct economic losses (100 million RMB) (d), proportion of direct economic losses relative to GDP (%) (e) caused by typhoon disasters from 1989 to 2021.

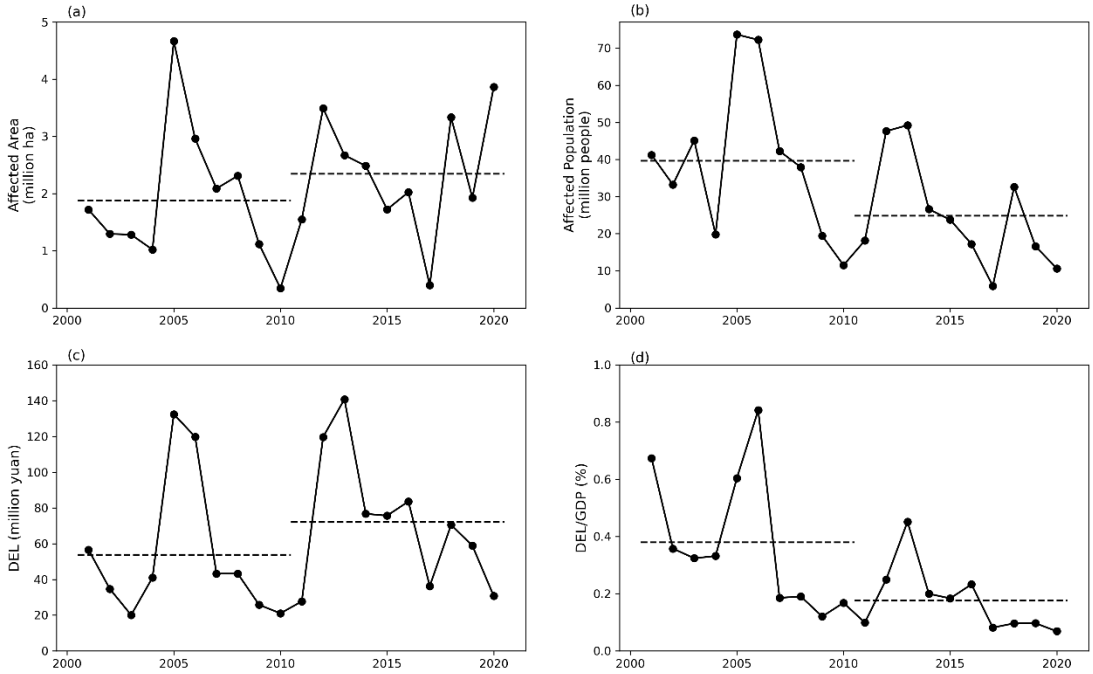

Fig. 2.23 Time series of (a) affected crop area, (b) affected population, (c) DEL, and (d) the ratio of DEL to GDP, caused by TCs during 2001–2020. The straight dashed lines denote the average values for the period of 2001-2010 and 2011-2020, respectively.